International Journal of Biological Macromolecules 322 (2025) 146804

Contents lists available at ScienceDirect

International Journal of Biological Macromolecules

journal homepage: www.elsevier.com/locate/ijbiomac

# PHA/PBAT biocomposites reinforced with rice straw lignocellulosic macromolecules: Decoding structure-property relationships through filler size and concentration

Laura Cabrera-Villamizar [a], Eugenia Núñez [a,b], Alcira Reyes [a,b], Erlantz Lizundia [c,d], Amparo López-Rubio [a,b], María José Fabra [a,b,*]

[a] Food Safety and Preservation Department, Institute of Agrochemistry and Food Technology (IATA), CSIC, Carrer del Catedràtic Agustín Escardino Benlloch, 7, 46980, Valencia, Spain
[b] Interdisciplinary Platform for Sustainable Plastics towards a Circular Economy – Spanish National Research Council (SusPlast), CSIC, Madrid 28006, Spain
[c] Life Cycle Thinking Group, Department of Graphic Design and Engineering Projects, Faculty of Engineering in Bilbao, University of the Basque Country (UPV/EHU), Bilbao 48013, Spain
[d] BCMaterials, Basque Center for Materials, Applications and Nanostructures, UPV/EHU Science Park, Leioa 48940, Spain

ARTICLE INFO

*Keywords:*
Rice straw
PHBV
PBAT
Composite
Valorization
Sustainability

ABSTRACT

The environmental crisis caused by the accumulation of conventional plastics requires the development of sustainable alternatives. This study introduced a novel approach to valorize agricultural waste by engineering composite materials based on blends of poly(3-hydroxybutyrate-*co*-3-valerate) (PHBV) and polybutylene adipate terephthalate (PBAT) reinforced with rice straw (RS) as a possible alternative to conventional plastics. Composites were produced by melt compounding and compression molding, varying PHBV:PBAT mass ratios (80:20, 50:50, 20:80), RS particle sizes (≤250 μm and ≤ 500 μm), and RS concentration (20, 30 and 40 *w*/w %). Results showed that the polymer ratio and RS particle size significantly affected filler dispersion and film properties. Smaller RS particles and higher PHBV content (80:20) led to better homogenization, improved interfacial adhesion, and enhanced water vapor barrier properties, while 50:50 blends showed poor dispersion and higher permeability. Colorimetric analysis highlighted the role of RS size in composite coloration. FTIR confirmed that RS interacts physically with the polymers, not chemically. RS addition increased rigidity and water contact angle but reduced ductility, thermal stability, and crystallinity (depending on the concentration and particle size), and increased water vapor permeability. Disintegration tests revealed that only 80:20 blends met ISO 20200:2016 standards, while biodegradation, under industrial composting, was lower for RS-containing blends than controls, highlighting the role of environmental conditions and microbial communities. Life cycle assessment showed the composites had a *cradle-to-grave* climate change impact of 7.89–8.28 kg $CO_2$-eq·$kg^{-1}$, which is lower than commercial plastics. These findings demonstrate the potential of rice straw as a sustainable filler for biodegradable PHBV/PBAT composites, offering promising alternatives for eco-friendly packaging applications.

## 1. Introduction

The valorization of rice straw (RS) has attracted significant research interest in recent years. The global RS production is estimated to be between 740 and 1170 million tons annually [1], highlighting the need of effective utilization strategies for this abundant agricultural residue. In Spain, rice (*Oryza sativa*) production is dominated by *japonica* and *indica* varieties [2]. A typical disposal practice is burning, which generates toxic gases with greenhouse gas potential and results in the loss of potentially usable biomass that could be repurposed. Therefore, circular economy approaches are needed to mitigate the environmental impact and provide alternative solutions that utilize RS as a raw material for various processes and products. The low density and the richness in several components of RS have promoted its application as a lower-

* Corresponding author at: Food Safety and Preservation Department, Institute of Agrochemistry and Food Technology (IATA), CSIC, Carrer del Catedràtic Agustín Escardino Benlloch, 7, 46980, Valencia, Spain.
*E-mail addresses:* la.cabrera10@iata.csic.es (L. Cabrera-Villamizar), enunez@iata.csic.es (E. Núñez), alcira.reyes@iata.csic.es (A. Reyes), erlantz.liizundia@ehu.eus (E. Lizundia), amparo.lopez@iata.csic.es (A. López-Rubio), mjfabra@iata.csic.es (M.J. Fabra).

https://doi.org/10.1016/j.ijbiomac.2025.146804
Received 9 June 2025; Received in revised form 5 August 2025; Accepted 11 August 2025
Available online 12 August 2025

carbon building material [3], a source of nanocellulose and nano-hemicellulose [4], and as a lignin-silica hybrid adsorbent for contaminant removal [5], among others. The complex composition of RS enables the extraction of valuable components, including cellulose (which can be used in films, absorbents, biosensors, and bioplastics), hemicelluloses (as precursors of xylitol and xylooligosaccharides), and lignin (with application as fertilizers, antimicrobials, hydrogels and UV-light shielding), among others [6]. Although RS is a source of various valuable compounds, its direct incorporation as a filler in composite materials presents a more economical and energy-efficient alternative. This approach reduces material costs and waste streams generated during processing by simply milling and adding the RS to a polymer matrix. Several studies have explored incorporating RS into various polymer matrices, including polypropylene (PP) and high-density polyethylene (HDPE) [7], polyvinyl alcohol (PVA) [8], polylactic acid (PLA) [9], polyvinyl chloride (PVC) [10], polyethylene (PE) [11], starch [12], and natural rubber [13]. However, the use of certain biopolyesters which are of emerging relevance in the packaging field, such as polyhydroxyalkanoates (PHAs) and polybutylene adipate terephthalate (PBAT) as polymer matrix in RS composites remains unexplored. This study addresses this gap by investigating the development of novel composite materials based on RS and blends of poly(3-hydroxybutyrate-*co*-3-valerate) (PHBV) and PBAT. On the other hand, not only is the percentage of the filler relevant, but the particle size might tremendously influence its interaction within a polymer matrix, which has been understudied [14]. The particle size of the RS filler altered the physical presentation and accessibility to the RS macromolecules (cellulose, hemicellulose, and lignin). For instance, a larger surface area would allow better interfacial adhesion with the polymer matrix, improving mechanical properties [1]. Also, the mechanical grinding of lignocellulosic particles can reduce cellulose crystallinity, decrease their average molecular weight, and cause structural changes [15]. Thus, it is possible that the smaller particles improved dispersion but might not provide the same reinforcement as larger ones. On the other hand, one important effect when using fibrous fillers as reinforcing agents, as RS, is the aspect ratio (length-to-diameter ratio). In this case, the desirable reinforcement particles are generally longer and thinner fibrils; however, if grinding is too severe, it leads to very short particles, and the reinforcing effect can be reduced; meanwhile, the larger particles integrity is better preserved, and the reinforcing effect would be more noticeable [16]. Nevertheless, incorporating larger particles might generate agglomeration/aggregation within the composites, leading to weak points that appear to reduce the ductility and reinforcing properties [17].

PHBV, a type of PHA, is a bacterially-synthesized polyester and a leading candidate for biodegradable plastic production due to its favorable thermal and mechanical properties [18]. While PHAs are considered among the most promising thermoplastic biopolymers for biodegradable applications, the inherent brittleness of pure PHBV can limit its direct use [19]. Researchers have explored blending PHBV with other polymers, incorporating additives, or using plasticizers to mitigate this. PBAT, while not naturally derived, is a biodegradable polymer that can enhance the toughness and processability of PHBV when incorporated into composite formulations [20]. This combination offers a potential pathway to fully biodegradable materials.

Despite the clear benefits of using organic waste such as RS to make packaging materials, it results essential to implement standardized environmental metrics that enable a comparison on the potential sustainability of the new materials being developed with that of conventional materials. Accordingly, life cycle assessment (LCA) methodology is gaining relevance because it allows the determination of environmental impacts in multiple categories regarding the complete or specific life-cycle phase of a material or product [21–23]. The information acquired can be used to compare the environmental impacts with benchmark materials as well as to identify where the largest burdens of the materials are located (i.e., environmental hotspot identification) [24]. Next, eco-design strategies could be applied to further reduce the environmental footprint [25].

Consequently, this study aimed to develop composite biodegradable materials with PHBV-PBAT-RS by melt compounding and compression molding, evaluating the PHBV:PBAT ratio in the polymer blend (80:20, 50:50, and 20:80), the RS particle size ($\leq$ 250 μm or $\leq$ 500 μm), and the percentage of RS incorporated (20, 30, and 40 %). The polymeric blend ratios were chosen to better understand the behavior of the RS when used as a filler in various polymeric formulations; thus, focusing on the development of rigid-to-flexible materials and on understanding the interaction between different polymer ratios and the RS. These composite materials could lead to significant advancements in the development of biopolymeric materials by understanding the impact of RS as a filler, the impact of the PHBV-PBAT mixtures, as well as the different functionalities and physicochemical properties. Additionally, the study aimed to evaluate the effect of the different variables on the disintegration capacity of the films. Hypotheses include that adding PBAT would facilitate the processing of the mixtures by melt compounding and improve the flexibility of the materials. Furthermore, the incorporation of RS might improve the mechanical properties of the formulations but may impact the thermal stability of the materials; however, the impact on polymer melting and crystallization, as well as the effect on the disintegration performance, biodegradability and the environmental impact of the material (measured by life cycle assessment -LCA-), is yet unknown. Therefore, this study offers an advantage for biomaterial development, as it not only focuses on material formulation but also integrates a comprehensive evaluation of environmental performance. In addition, to developing composites based on PHBV, PBAT, and rice straw, key aspects such as disintegration, biodegradability and environmental impact were evaluated. This more holistic approach enables a through validation of the physicochemical properties and the sustainability of the materials, making it a complete and responsible approach to the development of new biomaterials.

The developed materials establish a foundation for creating PHA-based composites through the valorization of agricultural residues, thereby opening new opportunities for applications in agro-industrial and food packaging sectors.

## 2. Materials and methods

Fig. 1 displays a schematic overview of experimental design and methodology carried out in this work. It illustrates the development process followed, which included the incorporation of rice straw as fillers into bioplastic matrices. As shown, the formulation process covers a wide range of variables, as well as the film formation parameters, and the material characterization.

### 2.1. Materials

RS was sourced from a local producer in Sueca (Spain) in September 2021. The RS was left to dry in open fields and subsequently milled using 3.0 mm and 1.5 mm mesh screens. The milled material was stored in a desiccator containing silica gel to prevent moisture sorption. The RS was then sieved through two different mesh sizes ($\leq$ 250 and $\leq$ 500 μm) to evaluate the effects of particle size on the composite materials. The poly (3-hydroxybutyrate-*co*-3-hydroxyvalerate) (PHBV) employed in this study was obtained under the commercial reference PHI 002 (Nature-Plast SAS, France) and contained 1–2 % valerate according to the provider. The polybutylene adipate-*co*-terephthalate (PBAT) was also acquired from the same supplier under the commercial reference PBE 006.

### 2.2. Methods

#### 2.2.1. RS particle characterization

After drying and milling the RS to particle sizes of 3 mm and 1.5 mm, the moisture content was determined by placing the material in a forced

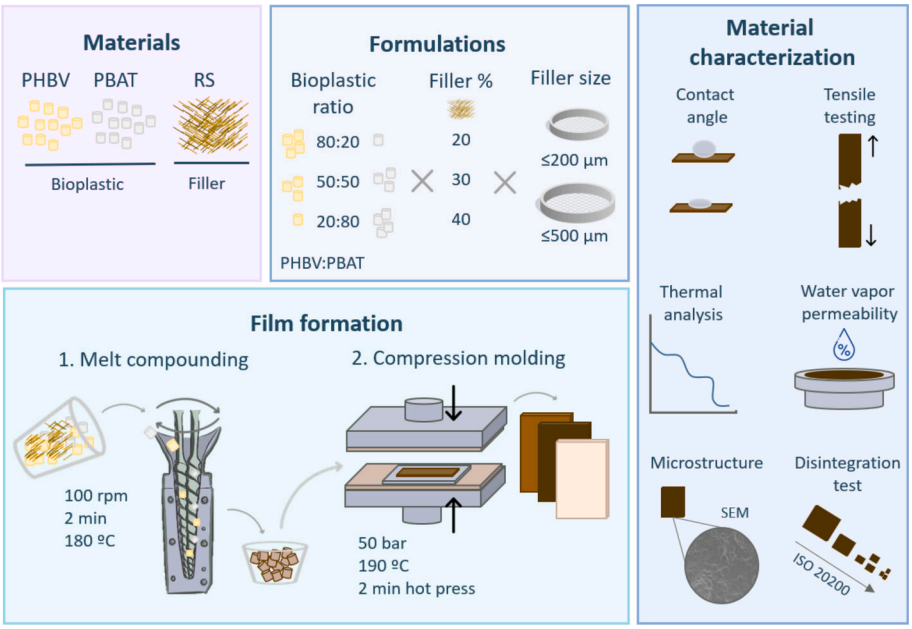


**Fig. 1.** Schematic overview of experimental design and methodology.

convection desiccation oven (J.P. Selecta, Spain) at 105 °C during 2 h. The mass difference before and after drying was recorded. Additionally, the particle size distribution was assessed using a sieving machine AS 200 (Retsch GmbH, Germany) with a series of sieves sizes (1000, 500, 250 and 125 µm). An in-depth characterization of the RS was conducted in a previous study by Cabrera-Villamizar et al. (2024) [26].

### 2.2.2. Preparation of composites by melt compounding

Prior to melt compounding, the RS was dried for 2 h at 105 °C to remove moisture and prevent polymer degradation by hydrolysis. The biopolymers PHBV and PBAT, were also dried at 60 °C for 2 h. The dried materials were weighed and stored in a desiccator to prevent moisture absorption until further processing. The biopolymers and the RS were incorporated simultaneously in the micro-compounder (Xplore 15HT, Netherlands) equipped with co-rotating screws and mixed for 2 min at 180 °C at a speed of 100 rpm. Following this, the obtained materials were extruded and manually collected and cut into pellets for further processing.

### 2.2.3. Compression molding

Films with thicknesses of 513 ± 24 µm were obtained by compression molding using a hydraulic press (Carver 4122, USA). The press was programmed to perform a preheating phase of 2 min at 190 °C, followed by a pressing phase at 50 bar for an additional 2 min at 190 °C. After pressing, the films were extracted immediately and placed on a smooth surface to cool down at room temperature (22 ± 2 °C).

### 2.2.4. Colorimetric analysis

The color parameters of the films were determined using the spectrophotometer CM26dG (Konica Minolta, Japan), based on the methodology described by Freitas et al. (2023) [27]. The color coordinates L* (lightness), a* (redness-greenness), and b* (yellowness-blueness) were obtained from the reflection spectra of the samples using D65 illuminant/10° observer. The total color differences (ΔE) were obtained using the following equation:

$$\Delta E^{*} = \sqrt{(\Delta L^{*})^{2} + (\Delta a^{*})^{2} + (\Delta b^{*})^{2}} \quad (1)$$

where $\Delta L^{*} = (L^{*} - L^{*}_{0})$; $\Delta a^{*} = (a^{*} - a^{*}_{0})$: $\Delta b^{*} = (b^{*} - b^{*}_{0})$; being $L^{*}_{0}$, $a^{*}_{0}$ and $b^{*}_{0}$ the color coordinates of the controls of each polymer blend formulation. Thus, the color differences were used to compare each polymer blend formulations before and after the addition of the RS independently. The measurements were carried out in triplicate, and each replicate consisted of three subsamples. CIE-L*a*b* coordinates, Lightness ($L^{*}$), hue ($h^{*}_{ab}$) and chroma ($C^{*}_{ab}$) were obtained from the reflection spectra as reported by Cabrera-Villamizar et al. (2025) [28].

### 2.2.5. Contact angle

The contact angle was measured using a drop shape analyzer (DSA25S Krüss, Germany). The angle was recorded using distilled water at room temperature ~ 22 ± 2 °C. Two repetitive measurements were recorded 10 s after the drop was in contact with the film. The reported angles were the average of the droplets' right and left angles and the global average of 10 measurements of each composite.

### 2.2.6. Water vapor permeability (WVP)

The water vapor permeability of the films was determined using a modified version method described by Pérez-Bassart et al. (2023) [29]. Films were mounted between the upper (open O-ring) and lower aluminum components of a Payne permeability cup (3.5 cm diameter, Elcometer SPRL, Hermelle/s Argenteau, Belgium). A rubber O-ring placed between the film and the base of the cup ensured a hermetic seal. The cups, containing pre-dried silica, were then placed in a sealed glass container maintained at 75 % relative humidity (RH) and 23 ± 1 °C using a saturated sodium chloride solution. The cups were weighted using an analytical balance Precisa 520 (Precisa Gravimetrics AG, Switzerland) over time until stabilization was reached. Water vapor permeation rate and WVP were calculated according to Fabra et al. (2014) [30] using the thickness of the films measured from four random points in the same film with a digital micrometer (Starrett, USA). The tests were performed in triplicate.

### 2.2.7. Scanning electron microscopy (SEM)

Micrographs were acquired using a Hitachi S-48 electron microscope (Hitachi High-Technologies Corporation, Japan) at an accelerating voltage of 10 kV and a working distance of 8–16 mm. The films were analyzed on their cross-section after cryo-fracturing by immersion in liquid nitrogen. The samples were mounted on M4 aluminum specimen sample holders using carbon tape and sputter-coated with a gold-palladium mixture under vacuum prior to examination.

*2.2.8. Tensile testing*

Tensile properties, including tensile strength (TS), elongation at break (EAB) and Young's modulus (E), were determined using a universal testing machine 34TM-5 Dual Column Table Model (Instron, USA) following an internal method based on the UNE-EN ISO 527-3 standard. Prior to testing, films were conditioned at 53 % RH until equilibrium was reached. Specimens were then cut into rectangular strips with dimensions of 10 mm × 70 mm. Film thickness was measured four times along each sample before testing. The initial grip separation was 50 mm, and the crosshead speed was 50 mm/min. Tests were conducted in triplicate.

*2.2.9. Fourier Transform Infrared Spectroscopy (FTIR)*

FTIR spectroscopy analyses were conducted in attenuated total reflectance (ATR) mode utilizing a FT/IR-4000 Series equipment (JASCO, Japan). The films were positioned on the ATR crystal (ZnSe) for examination at ambient temperature of 22 ± 2 °C, with scan executed at a resolution of 4 $cm^{-1}$, across the spectral range of 4000–600 $cm^{-1}$ while averaging a total of 32 scans. Air served as the background reference. The experiments were carried out in duplicate.

*2.2.10. Thermogravimetric analysis (TGA)*

The thermal stability of the films was evaluated using the thermogravimetric analyzer TGA 550 (TA Instruments, USA). The specimens, weighing between 6 and 9 mg, were subjected to a heating ramp from 50 °C to 850 °C at a rate of 10 °C/min under oxidative atmosphere (air). Derivative thermogravimetric curves (DTG) were employed to illustrate weight loss events that took place during the heating program. The analysis was conducted in duplicate.

*2.2.11. Differential Scanning Calorimetry (DSC)*

DSC thermograms were recorded using a DSC Q2000 instrument (TA Instruments, USA) to characterize the thermal transition of the developed composites. Samples of approximately 10 mg were analyzed in 50 μL aluminum pans with pierced lids under a nitrogen atmosphere. The samples were first heated at 10 °C/min from −50 to 200 °C and were kept at 200 °C for 2 min to erase the thermal history. A cooling scan at 5 °C/min from 200 to −50 °C followed and finally, a second heating scan at 10 °C/min from −50 to 200 °C was performed. The obtained ΔH was normalized considering the mass percentage of the polymer phase in the composite, assuming that the RS filler does not show any thermal transition along the temperature ranges where polymer melting and crystallization take place. Likewise, the melting enthalpies of PHBV and PBAT were integrated together as they appeared unresolved in the thermograms. Duplicate measurements were performed on each film.

*2.2.12. Disintegration assay according to ISO 20200:2016*

The disintegration of the tested films was assessed according to ISO 20200:2016 standard, which outlines a laboratory-scale composting test for determining the disintegration degree of plastic materials. A synthetic composting substrate was prepared by mixing 40 % sawdust, 30 % rabbit feed, 10 % mature compost, 10 % corn starch, 5 % sucrose, 4 % corn oil, 1 % urea and water, mimicking the conditions of a controlled composting environment. The test was conducted in triplicate, with each replicate consisting of a propylene container (30 cm × 20 cm × 10 cm) filled with 10 g of film sample and 1000 g of the prepared synthetic composting substrate. The films were cut from hot pressed films (10 mm × 10 mm × 0.2 mm). The substrate was maintained at 55 % moisture content throughout the 90-day incubation period at controlled temperature 58 ± 2 °C. Substrate moisture and total container weight were monitored regularly, water was added when required to compensate any loss of moisture. After 90 days, the disintegration degree was determined by sieving the composted material through a series of sieves with 10 mm, 5 mm and 2 mm mesh sizes (according to ISO 3310-1). The non-disintegrated film fragments retained on the sieves were collected and weighted using an analytical balance Precisa 520 (Precisa Gravimetrics AG, Switzerland). The disintegration degree was then calculated based on the mass loss of the initial film sample. The following equation was used for this calculation:

$$D_{j=\frac{m_i-m_r}{m_i}\times 100} \quad (2)$$

where $D_j$ express the disintegration degree, $m_i$ the initial dry mass, and $m_f$ the dry mass of the test material recovered at different incubation stages [31].

*2.2.13. Biodegradation*

Biodegradation of the film samples was assessed according to ISO 14855-2:2019 standard, which specifies a method for determining the ultimate aerobic biodegradability of plastic materials under controlled composting conditions by measuring evolved carbon dioxide $CO_2$ using a gravimetric technique. A mature, stabilized compost was used as the inoculum mixed with 320 g of sand as an inert material and sufficient water to achieve 65 % moisture content. The materials to be tested were films with thickness of 1 mm and dimensions of 10 mm × 10 mm and were added to the inoculum. This mixture was placed in a 3 L static reactor and incubated under aerobic conditions at 58 ± 2 °C for six months (for industrial compost) and at 30 ± 2 °C for one year (for home compost) analyses. Aerobic conditions were maintained by continuously pumping $CO_2$-free air into the reactors. Manual agitation once a week ensured homogeneous air distribution within each reactor.

The experiment consisted of three reactor types, each three replicates: (i) a blank control containing only compost, (ii) a positive control using cellulose as a reference material, and (iii) reactors containing the film samples. The emitted $CO_2$ was trapped in a soda lime column, and the absorbed $CO_2$ mass was measured gravimetrically using an analytical balance Mettler Toledo (ME 204220 g/0.1 mg). The percentage of biodegradation was calculated as the ratio of $CO_2$ emitted from the test sample to its theoretical maximum amount of $CO_2$ ($ThCO_2$) that can be produced from the test material.

*2.2.14. Life Cycle Assessment (LCA)*

The life cycle assessment (LCA) methodology as guided by the international standards ISO 14040/14044 has been implemented to the complete life-cycle of the composite films to account for their potential environmental sustainability. The study adopted a *cradle-to-grave* system boundary, considering the raw material sourcing with its related upstream processes, electricity needs for film production, waste management, end-of-life treatment and the related emission of fossil $CO_2$ during the final stage. A zero-burden approach is taken for the rice straw and solely its transport to the processing site and conditioning (e.g. drying, grinding) is included in the inventory. The life cycle inventory has been modeled according to primary data from laboratory-scale experiments (Fig. S1, Table S1). To meet Europe's renewable energy targets (Renewable Energy Directive EU/2023/2413), a medium-voltage electricity mix (that corresponds to 1–24 kV, medium to small scale industry, service sector and public buildings) has been utilized. The modeling was conducted using the latest update of Ecoinvent (ecoinvent v3.11 Cut-Off Unit Processes, released on December 2024), in combination with the PEF Database 3.1. The OpenLCA 2.4.0 software together with the Environmental Footprint v3.1 life cycle impact assessment methodology was utilized for the calculations. The functional unit was set at 1 kg of film to enable comparison. Benchmark materials were modeled according to the following entries:

- Polypropylene production, granulate | polypropylene, granulate | Cutoff, U – RoW + extrusion, plastic film | extrusion, plastic film | Cutoff, U – RoW.
- Polyethylene terephthalate production, granulate, bottle grade | polyethylene terephthalate, granulate, bottle grade | Cutoff, U – RoW + extrusion, plastic film | extrusion, plastic film | Cutoff, U – RoW.

- Packaging film production, low density polyethylene | packaging film, low density polyethylene | Cutoff, U – RoW.
- Polylactic acid production, granulate | polylactic acid, granulate | Cutoff, U – GLO + extrusion, plastic film | extrusion, plastic film | Cutoff, U – RoW.
- Polyvinyl chloride production, unspecified polymerization, weighted average | polyvinyl chloride, unspecified polymerization, weighted average | Cutoff, U – RoW + extrusion, plastic film | extrusion, plastic film | Cutoff, U – RoW.

#### 2.2.15. Statistical analysis

To evaluate significant differences among the treatments, a one-way analysis of variance (ANOVA) was performed. Assumptions of normality and homogeneity of variance were checked prior to conducting the ANOVA. Following a significant ANOVA result, a Tukey's Honestly Significant Difference (HSD) post-hoc test was used to determine which specific treatment groups differed significantly from each other. Statistical analyses were conducted using Statgraphics Centurion 19 × 64 software (Statgraphics Technologies, USA). A significance level of $\alpha = 0.05$ was used for all statistical tests.

## 3. Results and discussion

### 3.1. RS characterization

RS composition was determined in a previous study from the same group. The different detected components were: lignin (22 %), lipids (5 %), ashes (16 %), proteins (6 %) and carbohydrates (44 %) [26]. The moisture analysis of RS revealed an initial water content of 8.53 ± 0.33 %. Consequently, the residue was dried before the melt compounding process to prevent phase separation, which could result in a heterogeneous mixture, and to mitigate polymer hydrolysis reactions that could lead to degradation, thereby reducing the molecular weight and deteriorating the mechanical properties of the final material [32]. Composite formulations were developed using two different particle sizes of the RS and its impact on the physicochemical properties was investigated. As shown in Fig. 2, after grinding and sieving the rice-derived residue, the majority of the particles were below 250 μm. Therefore, a particle size of ≤250 μm was selected for further processing. Additionally, to assess the impact of particle size on the composite development, composite films were also developed using RS with a particle size of ≤500 μm, as an example of less processed material. Previous studies have explored the effect of torrefied larch and yellow poplar biomass particle size in the composite formulation without significant effects regarding the mechanical properties [33]. In the present study, an in-depth analysis of the particle size effect in the composite properties was performed.

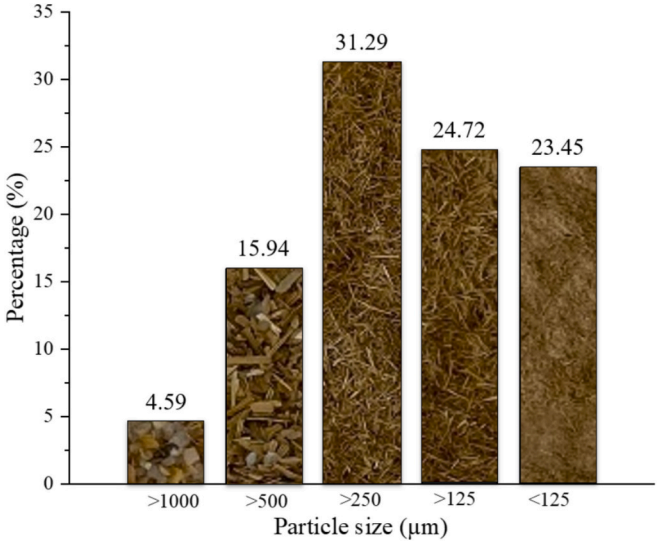


**Fig. 2.** Particle size distribution of RS, illustrating the percentage of particles in five size fractions. The image in the bars show the different particle types presented in the sieved material after milling.

### 3.2. Optical properties

As shown in Fig. 3, the composite materials obtained after melt compounding and compression molding exhibited opaque and smooth surfaces. The control samples showed a light-yellow color, and the composite films showed different shades from light to dark brown. The evidenced color was related to the intrinsic color of the milled RS. As expected, the materials with RS, at both particle sizes (≤ 250 μm and ≤ 500 μm), showed distinct colorimetric variations when compared to their control blends. These color variations can be attributed to the distribution and organization of the RS particles within the polymeric matrix. In this respect, previous reports have described that the addition of fillers can influence the final color of the composite through various mechanisms and change other physicochemical properties of the materials. For instance, the addition of graphene as filler in high concentrations might lead to particle aggregation, impacting the tensile strength of the materials [34].

To quantify color changes within each polymeric blend, the color difference (ΔE*), lightness difference (ΔL*), chroma difference (ΔC*), and hue difference (ΔH*) were calculated relative to the control films (0 % RS) for each polymer ratio (Table 1). The color difference (ΔE*) significantly increased with increasing RS percentage, with higher RS loadings resulting in higher ΔE* values. This effect was more pronounced with smaller RS particle sizes (≤ 250 μm). For all PHBV:PBAT ratios, films with smaller RS particles (≤ 250 μm) exhibited higher ΔE* values compared to those with larger particles (≤ 500 μm) at the same RS concentration, indicating that smaller particles induced a greater color change. For example, in the 80:20 blend, the ΔE* for the 40 % RS loading was 57.94 ± 0.23 with the smaller particle size, compared to 56.45 ± 0.09 for the larger size. This suggests that the smaller particles facilitated a more homogeneous dispersion within the polymer matrix, leading to a more intense color modification. Similarly, ΔL* values indicated that RS addition darkened the films compared to the control, with a direct correlation between RS loading and darkness. A notable effect of RS particle size on the colorimetric properties was observed, with a clear increase in ΔE* with higher RS content, confirming that increasing the RS concentration led to a more pronounced color change in the blends. The chroma difference (ΔC*) showed that films became duller with 30 % or 40 % RS addition, particularly with smaller particle sizes (≤ 250 μm) and in the 80:20 polymer blend. However, with 20 % RS and polymer ratios of 50:50 and 80:20, the films showed positive values, indicating brighter colors in contrast to higher loads. Finally, the hue angle difference (Δh*) confirmed that the control films lacked color tone purity, while RS-containing formulations exhibited more distinct color tones.

### 3.3. Contact angle

The hydrophobicity of the films, indicated by the water contact angle (WCA), was also determined, and the results are depicted in Fig. 4. The control blends did not show significant differences, demonstrating that the PHBV:PBAT ratios did not affect the surface hydrophobicity of the materials. On the other hand, after adding the RS as filler, there were significant effects, especially at 80:20 formulation with the higher RS% incorporated (40 %). The results highlight the significant influence of the PHBV: PBAT blend on the final hydrophobicity of the composite. At 80:20 ratio, shown in Fig. 4A, the addition of RS increases the WCA, improving the material's hydrophobicity. Specifically, with the ≤250 μm RS particles, the WCA appears to increase more substantially at 30 % and 40 % RS concentrations compared to the ≤500 μm particles at the

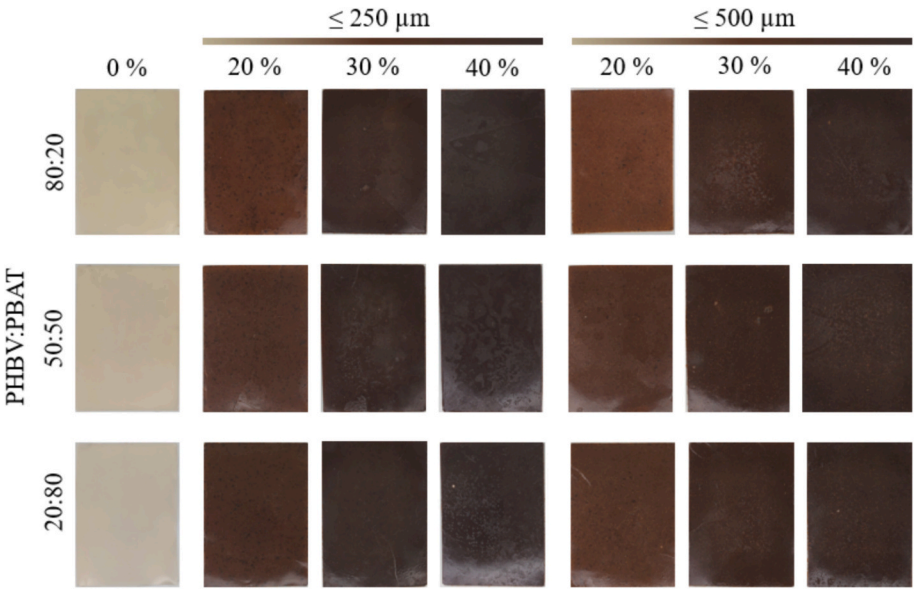


**Fig. 3.** Macroscopic appearance of the films, illustrating the influence of polymer ratios, particle size, and RS content. The specimens were recorded under the same light conditions to offer a better understanding of their appearance. As seen, the color differences were evident macroscopically; consequently, the colorimetric analysis enhances the comprehension of appearance.

**Table 1**
Effect of RS incorporation on the color of PHBV/PBAT blends. Films were prepared with varying RS content (0–40 %) and particle size (≤ 250 µm and ≤ 500 µm) at PHBV: PBAT blends of 80:20, 50:50, and 20:80. Color difference (ΔE), lightness difference (ΔL*), chroma difference (ΔC*) and hue difference (Δh*) were calculated relative to the respective 0 % RS control for each ratio. Statistical significance was determined using ANOVA and Tukey's test for comparisons within each ratio.

| PHBV:PBAT *ratio* | *RS particle size* | *RS %* | *ΔE* | *ΔL** | *ΔC** | *Δh** |
|---|---|---|---|---|---|---|
| 80:20 | Control | 0 | 0.00 ± 0.00 $^{a}$ | 0.00 ± 0.00 $^{a}$ | 0.00 ± 0.00 $^{a}$ | 0.00 ± 0.00 $^{a}$ |
| | ≤ 250 µm | 20 | 48.42 ± 0.02 $^{b}$ | -47.41 ± 0.07 $^{c}$ | 0.68 ± 0.49 $^{a}$ | -33.34 ± 0.43 $^{c}$ |
| | | 30 | 55.19 ± 1.09 $^{c}$ | -54.43 ± 1.04 $^{d}$ | -6.85 ± 0.18 $^{d}$ | -33.69 ± 0.30 $^{c}$ |
| | | 40 | 57.94 ± 0.23 $^{d}$ | -56.97 ± 0.25 $^{e}$ | -9.39 ± 0.04 $^{e}$ | -33.87 ± 0.49 $^{c}$ |
| | ≤ 500 µm | 20 | 47.40 ± 0.19 $^{b}$ | -46.19 ± 0.32 $^{b}$ | 1.89 ± 0.36 $^{b}$ | -33.41 ± 0.24 $^{c}$ |
| | | 30 | 54.55 ± 0.19 $^{c}$ | -53.84 ± 0.17 $^{d}$ | -3.65 ± 0.32 $^{c}$ | -31.95 ± 0.30 $^{b}$ |
| | | 40 | 56.45 ± 0.09 $^{e}$ | -55.65 ± 0.11 $^{e}$ | -6.97 ± 0.29 $^{d}$ | -34.20 ± 0.42 $^{c}$ |
| 50:50 | Control | 0 | 0.00 ± 0.00 $^{a}$ | 0.00 ± 0.00 $^{a}$ | 0.00 ± 0.00 $^{a}$ | 0.00 ± 0.00 $^{a}$ |
| | ≤ 250 µm | 20 | 52.29 ± 0.04 $^{c}$ | -51.75 ± 0.04 $^{c}$ | -2.18 ± 0.24 $^{c}$ | -31.14 ± 0.11 $^{c}$ |
| | | 30 | 56.27 ± 0.07 $^{e}$ | -55.67 ± 0.06 $^{e}$ | -6.08 ± 0.02 $^{f}$ | -31.26 ± 0.19 $^{c}$ |
| | | 40 | 58.21 ± 0.06 $^{f}$ | -57.50 ± 0.07 $^{f}$ | -7.83 ± 0.02 $^{g}$ | -31.62 ± 0.35 $^{c}$ |
| | ≤ 500 µm | 20 | 51.16 ± 0.27 $^{b}$ | -50.53 ± 0.31 $^{b}$ | 1.30 ± 0.36 $^{b}$ | -30.96 ± 0.13 $^{c}$ |
| | | 30 | 54.61 ± 0.20 $^{d}$ | -54.06 ± 0.21 $^{d}$ | -3.15 ± 0.23 $^{d}$ | -29.82 ± 0.26 $^{b}$ |
| | | 40 | 56.35 ± 0.17 $^{e}$ | -55.79 ± 0.15 $^{e}$ | -5.10 ± 0.00 $^{e}$ | -31.29 ± 0.81 $^{c}$ |
| 20:80 | Control | 0 | 0.00 ± 0.00 $^{a}$ | 0.00 ± 0.00 $^{a}$ | 0.00 ± 0.00 $^{a}$ | 0.00 ± 0.00 $^{a}$ |
| | ≤ 250 µm | 20 | 53.12 ± 0.17 $^{c}$ | -52.78 ± 0.16 $^{c}$ | 1.21 ± 0.55 $^{b}$ | -27.04 ± 0.81 $^{c}$ |
| | | 30 | 57.00 ± 0.10 $^{e}$ | -56.75 ± 0.10 $^{e}$ | -2.84 ± 0.2 $^{e}$ | -28.31 ± 0.48 $^{cde}$ |
| | | 40 | 58.96 ± 0.10 $^{f}$ | -58.65 ± 0.10 $^{f}$ | -4.64 ± 0.37 $^{f}$ | -29.35 ± 0.63 $^{de}$ |
| | ≤ 500 µm | 20 | 50.88 ± 0.22 $^{b}$ | -50.29 ± 0.24 $^{b}$ | 3.45 ± 0.34 $^{c}$ | -25.24 ± 0.21 $^{b}$ |
| | | 30 | 55.39 ± 0.03 $^{d}$ | -55.13 ± 0.04 $^{d}$ | -0.64 ± 0.3 $^{a}$ | -28.21 ± 0.63 $^{cd}$ |
| | | 40 | 57.25 ± 0.18 $^{e}$ | -57.00 ± 0.19 $^{e}$ | -1.78 ± 0.24 $^{d}$ | -29.69 ± 0.22 $^{e}$ |

same concentrations. This suggests that smaller RS particles may be more effective in enhancing hydrophobicity at higher concentrations in this specific blend ratio. On the other hand, in the 50:50 blend shown in Fig. 4B, the increase of WCA was less pronounced with the addition of RS. While the trend was slightly increased, the differences were not significant. Furthermore, the effect of particle size was minimal in this

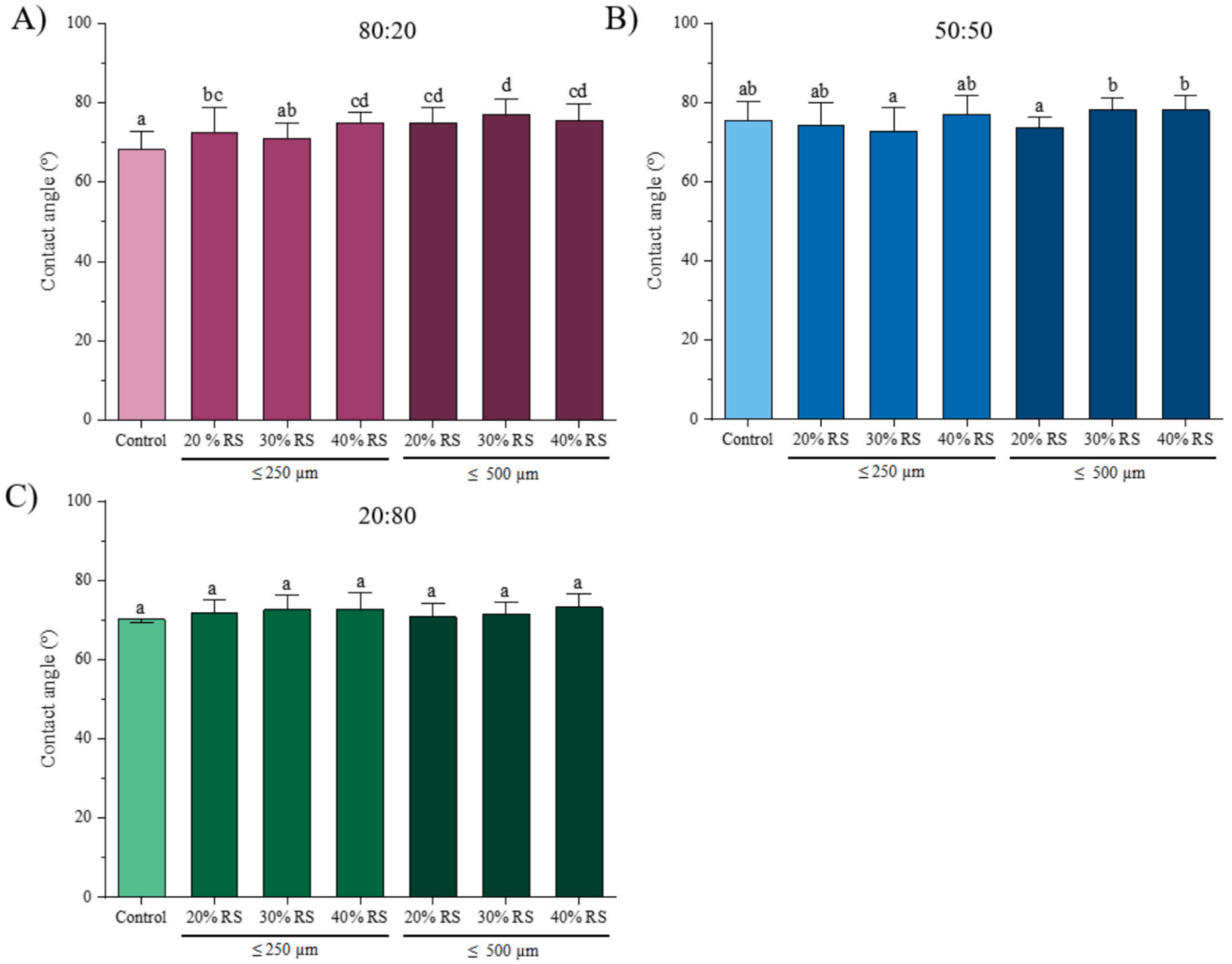


**Fig. 4.** Contact angles of PHBV-PBAT-RS films after compression molding. Ratios of PHBV:PBAT are (A) 80:20, (B) 50:50, and (C) 20: 80. Different letters indicate significant differences after an ANOVA test and Tukey-HSD test. Each statistical analysis was performed within each polymer ratio. The color code indicates the polymer ratio pink (80:20), blue (50:50) and green (20:80), and the color intensity represents whether the neat polymer or the particle size on each formulation.

blend. Similarly, for the blend of 20:80, the addition of RS did not show significant differences upon RS addition. The results showed the polymer ratios influenced the composite's final hydrophobicity and the way the filler was dispersed in the matrix. The 80:20 blend demonstrated the most significant improvement in hydrophobicity with RS addition, particularly with bigger particle sizes at higher concentrations and smaller particles with the highest concentration (40 %). On the other hand, as the PBAT content increased (50:50 and 20:80 blends), the effects of RS on WCA decreased, suggesting that the matrix composition plays a crucial role in how the filler influences the material's surface properties.

The observed surface behavior can be explained by the different microstructures generated when blending PHBV:PBAT. It has been reported that depending on the ratios of these polymers, the internal structures and polymeric interactions change tremendously. Particularly from scanning electron microscopy (SEM), differential scanning calorimetry (DSC) and dynamic mechanical analysis, it has been proven that PHBV and PBAT are naturally immiscible. Furthermore, when PHBV is more (70/30) or equally (50/50) abundant, it tends to form globules covered by PBAT; meanwhile, when PBAT is more abundant (30/70), the PBAT fraction forms a network throughout the PHBV in fine strands [35]. Additionally, as will be shown in Section 3.7.1., in the cross-section-SEM analyses, the blends showed the previously reported globular-like structures (shown as partially melted pellets interconnected physically between them but still differentiating two types of materials on the blend, looking like polymer inclusions within the other material), confirming the immiscibility between the polymers. On the other hand, it was observed that the different filler size affects the surface contact angle. Thus, the organization and distribution of the polymeric network influence the interaction with RS and, as observed, affect the surface properties. Additionally, the hydrophobization behavior of RS can be explained by the non-polar compounds present in its composition, including the non-soluble lignin and lipophilic compounds such as fatty acids, mono-, di-, and triglycerides, high molecular esters, tocopherols, sterols, among others [36]. Moreover, lignin's inherent hydrophobicity might reduce the wettability and water uptake of polymeric composites [37].

### 3.4. Mechanical properties

The mechanical behavior of the blends was expected to correlate with the polymer proportion. The rigidity and brittleness of the blends, analyzed through the Young's modulus (E) and elongation at break (EAB), displayed a trend of 80:20 > 50:50 > 80:20. This trend indicated

that higher rigidity and stiffness were associated with increased PHBV content in the formulation. Conversely, the ductility of the materials, assessed through tensile strain at break, exhibited the opposite trend 20:80 > 50:50 > 80:20, indicating that the addition of PBAT enhances the flexibility of the composites. The incorporation of RS significantly influenced the mechanical properties of the PHBV: PBAT blends, with effects dependent on the polymer blend ratio, RS particle size, and RS percentage incorporated. As expected, EAB generally decreased with increasing RS content across all blends and particle sizes, as shown in Table 2, indicative of increased stiffness due to the RS filler incorporation. Notably, the 20:80 blend, particularly with the smaller RS particle size (≤ 250 μm), exhibited a less pronounced reduction of 34 % in EAB compared to the other blends, suggesting a potentially more ductile composite. This is due to the higher proportion of PBAT which is commonly known for reducing brittleness of the PHBV/PBAT formulations in other composites while preserving the biodegradable properties in the formulations [38]. Conversely, Young's or Elastic Modulus showed a consistent and statistically significant increase (from 1 % up to 35 %) with RS addition across all blends and particle sizes, confirming the reinforcing effect of the RS as rigidity increased. This increase was substantially greater with the smaller RS particle size (≤ 250 μm), emphasizing the importance of good RS dispersion within the polymer matrix. The 80:20 blend exhibited the most significant increase (35 % in comparison with the control) in E, implying a stronger interaction or better compatibility between the RS and this specific blend ratio; correspondingly, the SEM analysis, as it will be discussed in Section 3.7., demonstrates that the 80:20 blend easily integrates the RS in contrast to the 50:50 formulation, thus, confirming the polymer-filler compatibility.

The effect of RS incorporation on tensile strength (TS) was more complex and dependent on both blend ratio and RS content. In the 80:20 blend, TS appeared to increase initially at 20 % RS, followed by a decrease at higher RS percentages (30 % and 40 %), suggesting an optimal RS content around 20 % for this blend. This decrease in TS at higher RS loadings is likely attributable to particle agglomeration or dispersion issues. This information was confirmed by previous authors, working with synthetic materials, who found that up to 20 % of fiber content, the tensile and bending strength of RS-polypropylene composite increased. However, tensile strength decreased on further loadings of RS fiber that was attributed to pool interfacial adhesion of RS with the polymer [6]. Likewise, the 50:50 blend showed a similar trend, albeit with a less pronounced decrease in TS after the initial increase. In contrast, the 20:80 blend, especially with smaller RS particles, showed a more gradual increase in TS with increasing RS content, without a clear decrease within the tested range. This suggests that the 20:80 blend may accommodate higher RS loadings without significant strength loss. These results highlight the potential of tailoring the PHBV: PBAT blend ratio and RS particle size to achieve desired mechanical properties for specific applications.

### 3.5. FTIR spectroscopy

The molecular changes in control films and films with added RS were examined using FTIR-ATR (4000–600 $cm^{-1}$) spectroscopy (Fig. 5 A-E). The neat polymers, control blends, and RS, shown in detail in Fig. 5A and B, showed the broad spectrum and the fingerprint region of the polymers, respectively. Particularly, in the neat polymer spectra the band associated with PHBV was the one at 1377 $cm^{-1}$ and the ones associated with PBAT at 726 $cm^{-1}$. On the other hand, the control blends showed these bands and a more related spectra to the PHBV neat material, which might be explained by its availability in the surface of the control blends. Nevertheless, the signal associated with PBAT at 726 $cm^{-1}$ was also clear in the control blends, mainly in the 20:80 ratio, as expected. In general, an absorption band at 1719 $cm^{-1}$ was observed and attributed to C═O ester stretching in both PHBV and PBAT [39], with band intensity varying with polymer ratio. Bands at 1454 and 1377 $cm^{-1}$ correspond to $CH_2$ and $CH_3$ bending vibrations in both polymers [40]. The 1264–1051 $cm^{-1}$ region, associated with C—O stretching, also varied with polymer ratio [41]. Bands at 974, 940, and 897 $cm^{-1}$, indicative of the amorphous phase of PHBV, were most prominent in the 80:20 formulation, as expected [42]. Bands at 868 and 825 $cm^{-1}$, associated with PHBV crystalline structures (Fig. S3), decreased in intensity with increasing PBAT content.

The band at 726 $cm^{-1}$ was assigned to aromatic C—H bending in PBAT [43]. Therefore, as can be seen in Fig. 5C-E, the band was less visible not only when reducing the PBAT concentration, but when adding the RS. Thus, a possible change in the aromatic region might be generated after the addition of PHBV and RS in the PBAT. The effect was evidenced even in the 80:20 formulation with lower PBAT content. Regarding the particle size, the addition of RS to the formulations resulted in a proportional decrease in band intensities across the spectra. The persistence of the same spectral features in the RS composites and

**Table 2**
Tensile properties of polymer blends and composite materials with RS. Tensile testing curves are included in the Fig. S2. Values with different superscript letters indicate significant differences as determined by ANOVA and Tukey test.

| *PHBV:PBAT ratio* | *RS particle size* | *RS %* | *Elongation at break (%)* | *Young's Modulus (MPa)* | *Tensile Strenght (MPa)* |
|---|---|---|---|---|---|
| 80:20 | Control | 0 | $3.93 \pm 0.30^{a}$ | $1259 \pm 68^{hij}$ | $24.77 \pm 0.66^{a}$ |
| | ≤ 250 μm | 20 | $2.59 \pm 0.08^{a}$ | $1467 \pm 58^{k}$ | $16.71 \pm 0.44^{b}$ |
| | | 30 | $1.24 \pm 0.07^{a}$ | $1843 \pm 334^{l}$ | $11.84 \pm 0.94^{cd}$ |
| | | 40 | $1.24 \pm 0.32^{a}$ | $1699 \pm 79^{l}$ | $10.14 \pm 1.29^{efg}$ |
| | ≤ 500 μm | 20 | $2.36 \pm 0.17^{a}$ | $1233 \pm 102^{ghi}$ | $16.43 \pm 0.16^{b}$ |
| | | 30 | $1.97 \pm 0.06^{a}$ | $1273 \pm 55^{hij}$ | $12.30 \pm 0.23^{cd}$ |
| | | 40 | $1.57 \pm 0.14^{a}$ | $1414 \pm 170^{jk}$ | $11.23 \pm 0.53^{de}$ |
| 50:50 | Control | 0 | $5.02 \pm 0.54^{a}$ | $1118 \pm 31^{fgh}$ | $17.05 \pm 0.97^{b}$ |
| | ≤ 250 μm | 20 | $2.98 \pm 0.34^{a}$ | $936 \pm 66^{e}$ | $11.97 \pm 0.89^{cd}$ |
| | | 30 | $2.37 \pm 0.26^{a}$ | $1080 \pm 72^{efg}$ | $10.35 \pm 0.70^{ef}$ |
| | | 40 | $1.59 \pm 0.16^{a}$ | $1249 \pm 148^{ghij}$ | $9.80 \pm 1.17^{ghij}$ |
| | ≤ 500 μm | 20 | $3.00 \pm 0.27^{a}$ | $988 \pm 66^{ef}$ | $12.93 \pm 0.60^{c}$ |
| | | 30 | $2.34 \pm 0.27^{a}$ | $929 \pm 67^{e}$ | $10.05 \pm 1.21^{fgh}$ |
| | | 40 | $1.73 \pm 0.11^{a}$ | $1337 \pm 81^{ijk}$ | $10.69 \pm 0.14^{ef}$ |
| 20:80 | Control | 0 | $382.47 \pm 63.41^{b}$ | $194 \pm 1^{a}$ | $8.78 \pm 0.14^{ijkl}$ |
| | ≤ 250 μm | 20 | $7.96 \pm 0.62^{a}$ | $375 \pm 34^{ab}$ | $8.72 \pm 0.25^{jkl}$ |
| | | 30 | $5.08 \pm 0.70^{a}$ | $478 \pm 13^{bc}$ | $8.18 \pm 0.57^{kl}$ |
| | | 40 | $3.22 \pm 0.55^{a}$ | $737 \pm 41^{d}$ | $9.12 \pm 0.64^{hijk}$ |
| | ≤ 500 μm | 20 | $9.20 \pm 0.84^{a}$ | $329 \pm 21^{ab}$ | $8.55 \pm 0.20^{kl}$ |
| | | 30 | $5.47 \pm 0.66^{a}$ | $429 \pm 22^{b}$ | $7.87 \pm 0.21^{l}$ |
| | | 40 | $3.78 \pm 0.30^{a}$ | $622 \pm 60^{cd}$ | $8.50 \pm 0.41^{kl}$ |

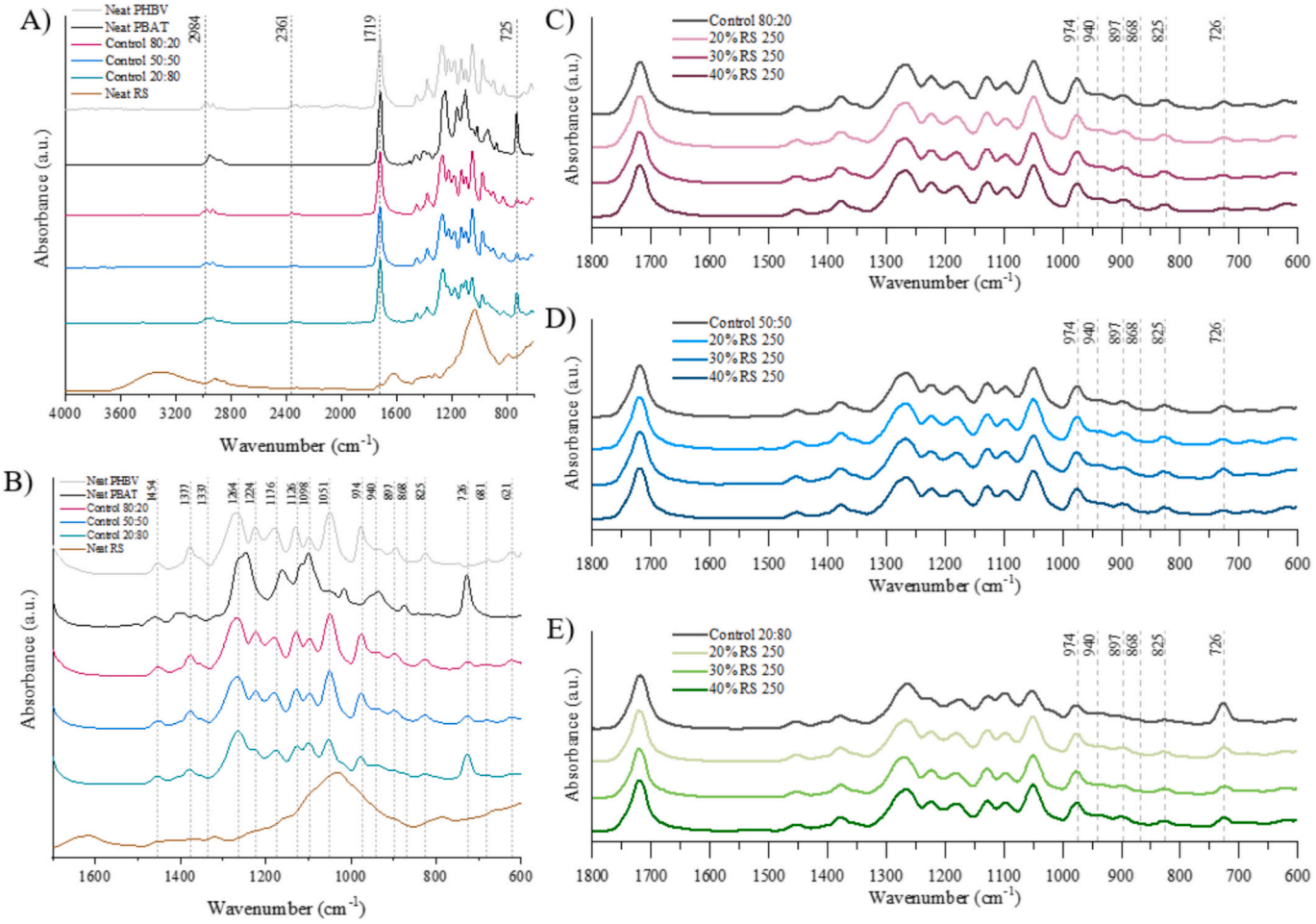


**Fig. 5.** FTIR-ATR spectra of the neat materials, control blends and biocomposites. Figs. A) and B) show the full spectra (4000–600 $cm^{-1}$) and the fingerprint region (1800–600 $cm^{-1}$), respectively, for the neat polymers (PHBV, PBAT), rice straw (RS), and control blends. Figs. C), D), and E) show the fingerprint region for biocomposites made with different PHBV/PBAT ratios (C: 80:20; D: 50:50, E: 20:80) and increasing percentages of rice straw (data shown for ≤250 μm particle size). The dotted vertical lines highlight the key absorption bands. Color coding differentiates the blend ratios pink for 80:20, blue for 50:50 and green for 20:80. In plots C)-E) a darker shade indicates a higher concentration of RS filler. Fig. S3 includes the spectra of the ≤500 μm particle composites.

the absence of RS associated bands, suggest that the interaction between PHBV, PBAT and RS is mainly based on physical dispersion and cohesion, rather than chemical interactions. Therefore, the FTIR results confirmed that the composite spectra are dominated by the typical features of the polymers, without spectra changes associated with the RS incorporation.

### 3.6. Thermal properties

As illustrated in Fig. 6, the thermogravimetric profile of the polymers underwent substantial alterations in comparison to both the control and the pure polymers, as anticipated. The pure PHBV exhibited a singular weight loss event from 246 to 305 °C with a maximum at 296.52 °C, with a 1 % ash content. This result aligns with previous findings that linked the presence of ashes with the addition of inorganic fillers, mineral fillers, nucleating agents, or stabilizers [44,45]. Notably, Zaidi & Crosky (2019) [46] reported a similar thermal behavior. Conversely, the PBAT degradation process exhibited a two-step weight loss; the first step between 292 °C and 408 °C with maximum at 373.53 °C and the second step between 430 °C and 530 °C with maximum at 497.45 °C. The initial weight loss, corresponding to 89.18 %, involved the thermal decomposition and oxidative degradation of the PBAT polymer. It has been observed that aliphatic segments of PBAT are particularly sensitive to oxidative degradation. This initial degradation is considered the primary decomposition of PBAT polymer chains [47]. Subsequently, the second weight loss of 11.34 % event with peak at 497.45 °C was likely associated with the decomposition and oxidation of more stable aromatic structures and char residues formed during the initial decomposition step [48]. In the control polymeric blends, a three-step weight loss process was identified, as evidenced by the presence of a single peak for PHBV degradation and additional PBAT degradation peaks (as shown in Table S2). The temperature of the first and second peaks increased in direct proportion to the amount of PBAT added to the control blends as shown in Fig. 5A. However, the third peak exhibited minimal variation in the control blends (80:20 (3.94 °C); 50:50 (4.48 °C); 20:80 (3.95 °C)). In contrast, samples containing RS (≤ 250 μm) exhibited a shift to lower temperatures and a decrease in the weight loss percentage associated with the PHBV thermal degradation, in contrast to the control ($T_1$), proportional to the percentage of RS utilized as a filler. It was observed that as the percentage of RS increased, the peak temperature decreased. This result indicates that the incorporation of RS led to a diminished thermal resistance of the composites, probably due to the interruption of intermolecular interactions in the polymer matrix as proposed by Tomato et al. (2022) [49] and Qin et al. (2022) [50]. This can be explained by the presence of residual moisture in the fillers which could hydrolyze ester bonds in both PHBV and PBAT at high temperatures during melt compounding. Additionally, the increase in ashes was proportional to the amount of RS added to the composites, reaching percentages up to 9 %. In detail, information regarding the degradation temperatures and weight losses is shown in Table S2. Similar thermal decomposition

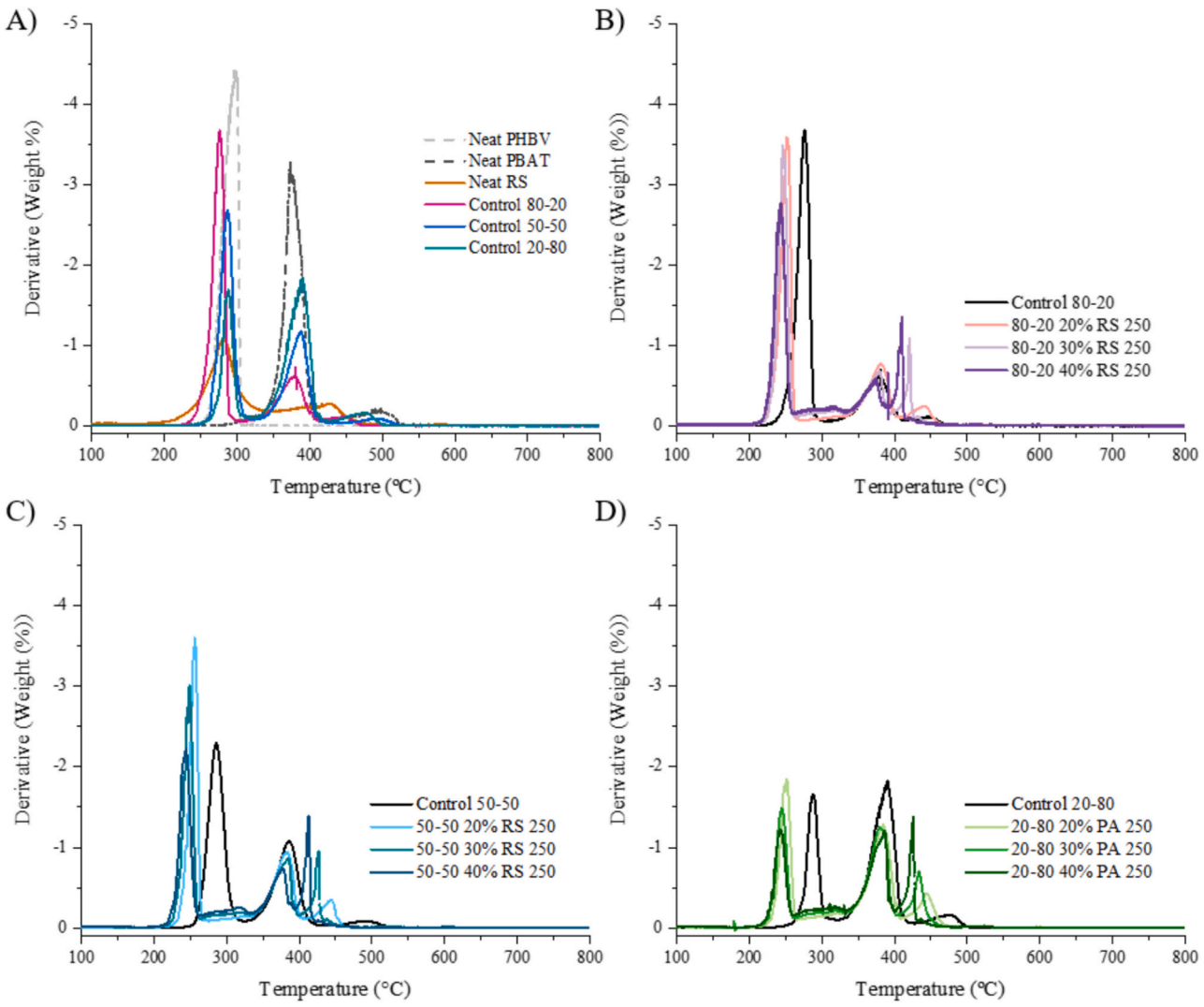


**Fig. 6.** DTGA curves of formulations with varying polymer ratios (PHBV: PBAT) and RS incorporation percentages (B—D), including controls (A). Data shown for ≤250 μm particles; see Fig. S4 for ≤500 μm. Color coding differentiates the blend ratios pink for 80:20, blue for 50:50 and green for 20:80, and darker shade indicates a higher concentration of RS filler.

characteristics were observed in the samples with ≤500 μm RS particle size, as shown in Fig. S4.

The DSC analysis provided valuable insights into the thermal behavior of PHBV: PBAT blends and the effect of the RS filler. Regarding the crystallization of the neat polymers, as shown in Fig. 7A, the PHBV showed the formation of crystals at ≈ 125 °C, while PBAT at ≈ 42 °C. Moreover, as expected, the associated enthalpy was higher for PHBV than the PBAT. Therefore, the crystallization enthalpy ($\Delta H_c$) decreased proportionally when the PHBV concentration was reduced. During the cooling step, the crystallization temperature ($T_c$) significantly varied and decreased proportionally with increasing PBAT content in the formulation (80:20: 109.5 °C; 50:50: 102.67 °C; and 20:80: 87.69 °C). As shown in Fig. 7B-D and Table 3, the effect of RS addition varied depending on the polymer ratio. The incorporation of RS in the 80:20 composites proportionally reduced the crystallization temperatures of the PHBV ($T_c$-PHBV), regardless of the particle size. Additionally, the $\Delta H_c$ presented the same tendency. On the other hand, in the 50:50 composites, there was the same tendency of reduction in the $T_c$-PHBV and reduction of the $\Delta H_c$, except the formula with the smaller particle size and 20 % of RS incorporated, which slightly increased the $T_c$ of the blend. Furthermore, the RS addition in the 20:80 composites demonstrated a less significant shift in the crystallization temperatures due to the lower content in PHBV. Nevertheless, regardless of the RS particle size, the same effect of $T_c$-PHBV and $\Delta H_c$ reduction was evidenced. Accordingly, the thermal properties of the polymeric blends were strongly influenced by the polymeric ratios and the RS concentration.

Furthermore, the melting temperatures ($T_m$), as shown in Table 4 and Fig. 7E-H, of neat PHBV and PBAT were ≈ 170 °C and ≈ 116 °C, respectively. The control blend 80:20 showed a cold crystallization event that was not recorded in the other blends or the neat polymers. In contrast, all the control blends showed two $T_m$-PHBV-associated temperatures, corresponding to the melting process of different PHBV crystals formed. During the analysis, the melting enthalpy was calculated by integrating together the peaks associated with PBAT and PHBV melting, since they were not resolved. The analysis of the 80:20 formulations showed that only $T_m$-PHBV-1 and $T_m$-PHBV-2 were recorded, as expected. In the $T_m$-PHBV-1, there were non-significant differences after incorporating the RS; meanwhile, in the $T_m$-PHBV-2, there were significant differences, and the $T_m$ was reduced after the RS addition, regardless of the particle size. Also, the RS incorporation decreased the $\Delta H_m$ values proportionally with the RS concentration. Similar findings were recorded for the 50:50 composites, where the $T_m$-PHBV-1 was slightly reduced after the RS incorporation. However, increasing the RS concentration showed a significant reduction of the $T_m$-PHBV-2 and $\Delta H_m$. This result indicates the formation of less stable polymeric crystalline structures due to RS particles or agglomerates hindering the

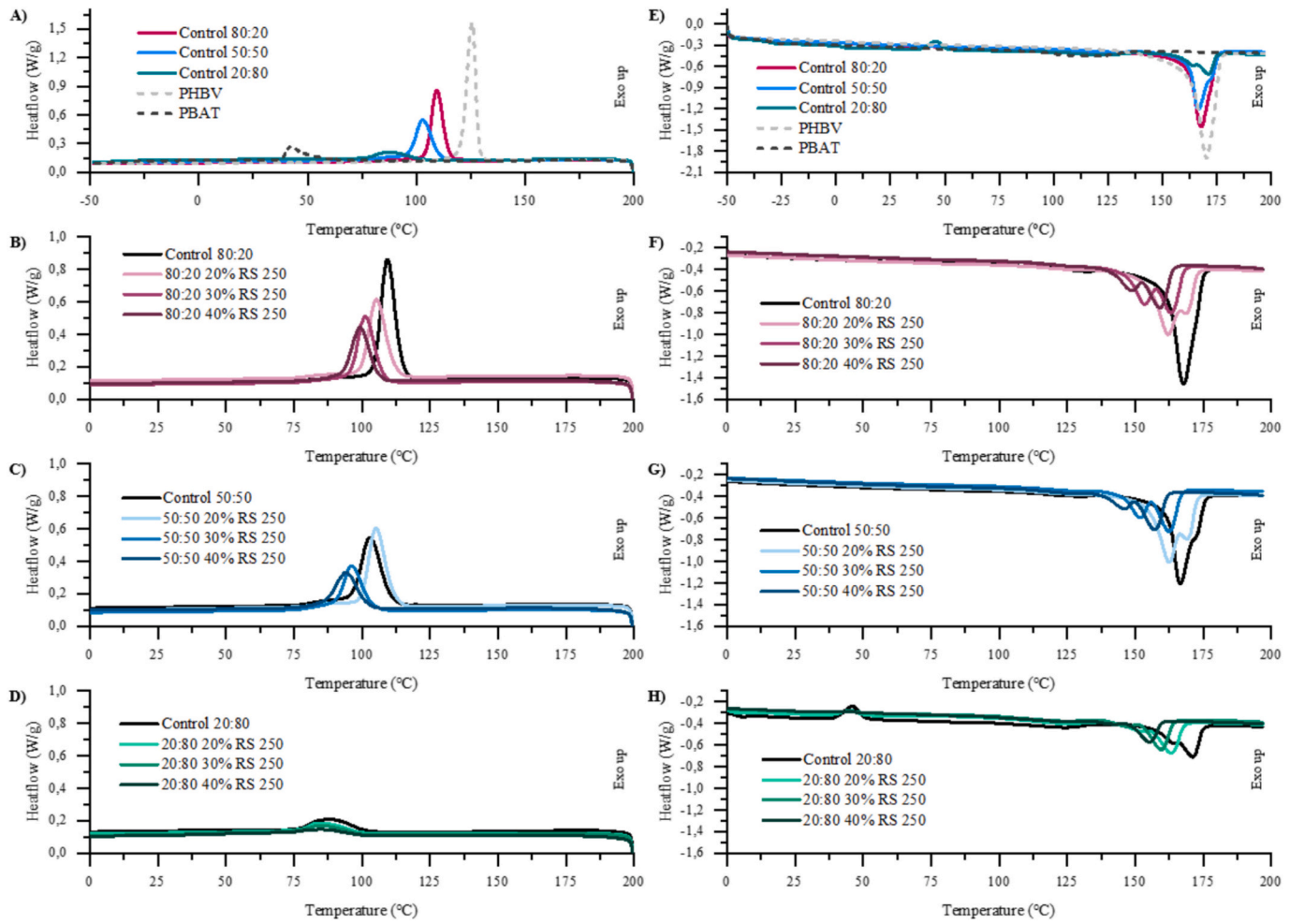


**Fig. 7.** DSC thermograms for particle size of ≤250 μm. A)-D) figures and E)-H) figures represents the cooling step and the second heating step, respectively. The composite thermograms are shown for each polymeric ratio. Thermograms of ≤500 μm are shown in Fig. S5. Color coding differentiates the blend ratios pink for 80:20, blue for 50:50 and green for 20:80, and darker shade indicates a higher concentration of RS filler.

crystallization process. Finally, the 20:80 composites showed the cold crystallization of the PBAT and the melting of the PHBV crystals. $T_{cc}$-PBAT showed the same temperature without significant differences, except for the ≤500 μm-40 % composite, which was slightly lower. On the other hand, the $\Delta H_{cc}$-PBAT showed a reduction proportional to the concentration of the RS regardless of the particle size. Thus, this demonstrated that the polymer ratio and the RS concentration influence the capacity of the polymers to crystallize and show a broad spectrum of crystallization profiles.

### 3.7. *In depth characterization of selected formulations*

While the high PHBV content formulations (80:20 and 50:50) exhibited suboptimal mechanical properties, their potential for enhanced biodegradability and sustainability warrants further investigation. These polymer blends, and those incorporating 40 % RS with a particle size of ≤500 μm, offer a significant opportunity to reduce reliance on petroleum-derived PBAT. Prioritizing PHBV, a bio-based polymer, and maximizing the incorporation of unprocessed RS, an abundant agricultural residue, aligns with the increasing demand for environmentally-friendly materials. This approach addresses the critical issue of plastic waste by promoting biodegradability and contributes to a circular economy through the valorization of agricultural byproducts. Therefore, despite the observed mechanical limitations, the promising environmental benefits of these formulations justify in-depth research and optimization, paving the way for sustainable alternatives to conventional petroleum-based polymers.

#### 3.7.1. *Morphological characterization of selected formulations*

The microstructure of the materials was analyzed using SEM (Fig. 8A). The 80:20 blend exhibited a continuous matrix with some irregularities. Higher magnifications revealed glomerular structures, consistent with PBAT incorporation, as reported by Zytner et al. (2023) [35]. The 80:20 control sample displayed a relatively homogeneous and compact polymeric matrix. However, the addition of 40 % RS resulted in a rougher and more heterogeneous structure. The RS particles were dispersed throughout the matrix, but interfacial adhesion appeared limited, with some voids and separation between the RS and the polymer blend. In contrast, the 50:50 blend showed a more porous and less cohesive structure, indicating immiscibility between the two polymers. With the addition of RS, this blend showed poor dispersion and deficient interfacial adhesion, characterized by larger voids and greater separation between the RS and the blend matrix.

These results were consistent with those previously discussed. For instance, the change in coloration when RS particles were added (particle size ≤500 μm) tend to be lower due to the generation of agglomerates. With regard to this, the SEM results suggest that while the presence of particle dispersion can be observed, the subsequent aggregation had the potential to influence the physiochemical properties of the composites. Such was the case of the mechanical properties, where RS dispersion played a crucial role. If the filler was less dispersed, as is the case with the 50:50 blends, the reinforcing effect of the RS was

**Table 3**
Crystallization analysis ($T_c$ and $\Delta H_c$) of polymers and composites by DSC during the cooling scan. The events observed correspond to the crystallization of PHBV phase, except in the pure PBAT sample. Values with different superscript letters indicate significant differences as determined by ANOVA and Tukey test. Blank cells indicate cases where the values information was not applicable or detectable.

| PHBV:PBAT ratio | RS particle size | RS % | $T_c$-PHBV (°C) | $\Delta H_c$ (J/g) |
|---|---|---|---|---|
| | Control | 0 | 109.50 ± 0.27 $^{b}$ | 63.24 ± 1.83 $^{b}$ |
| | | 20 | 104.90 ± 0.63 $^{c}$ | 39.78 ± 0.94 $^{d}$ |
| | ≤ 250 μm | 30 | 101.06 ± 0.08 $^{d}$ | 29.54 ± 0.12 $^{e}$ |
| 80:20 | | 40 | 99.03 ± 0.28 $^{e}$ | 21.59 ± 0.20 $^{fg}$ |
| | | 20 | 105.31 ± 0.20 $^{c}$ | 38.80 ± 1.45 $^{d}$ |
| | ≤ 500 μm | 30 | 101.64 ± 0.22 $^{d}$ | 29.48 ± 0.04 $^{e}$ |
| | | 40 | 98.99 ± 0.32 $^{e}$ | 20.58 ± 0.23 $^{fgh}$ |
| | Control | 0 | 102.67 ± 0.10 $^{d}$ | 46.58 ± 0.66 $^{c}$ |
| | | 20 | 105.15 ± 0.05 $^{c}$ | 39.93 ± 0.08 $^{d}$ |
| | ≤ 250 μm | 30 | 96.12 ± 0.13 $^{g}$ | 23.51 ± 0.35 $^{f}$ |
| 50:50 | | 40 | 93.70 ± 0.29 $^{g}$ | 17.82 ± 0.18 $^{gh}$ |
| | | 20 | 98.26 ± 1.26 $^{f}$ | 32.27 ± 0.31 $^{e}$ |
| | ≤ 500 μm | 30 | 95.49 ± 0.32 $^{fg}$ | 23.52 ± 0.00 $^{f}$ |
| | | 40 | 94.76 ± 0.30 $^{fg}$ | 16.73 ± 0.62 $^{ghi}$ |
| | Control | 0 | 87.63 ± 0.19 $^{h}$ | 15.79 ± 1.21 $^{hi}$ |
| | | 20 | 85.04 ± 0.62 $^{i}$ | 9.78 ± 2.28 $^{jk}$ |
| | ≤ 250 μm | 30 | 85.22 ± 0.17 $^{i}$ | 6.06 ± 0.26 $^{kl}$ |
| 20:80 | | 40 | 84.62 ± 1.03 $^{i}$ | 3,84 ± 0.17 $^{l}$ |
| | | 20 | 85.20 ± 0.01 $^{i}$ | 7,44 ± 0.24 $^{kl}$ |
| | ≤ 500 μm | 30 | 85.52 ± 0.62 $^{i}$ | 12,81 ± 1.13 $^{ij}$ |
| | | 40 | 84.25 ± 0.17 $^{i}$ | 7,02 ± 4.08 $^{kl}$ |
| Neat PHBV | – | – | 125.41 ± 0.23 $^{a}$ | 93,20 ± 1.15 $^{a}$ |
| | | | $T_c$-PBAT (°C) | |
| Neat PBAT | – | – | 42.24 ± 0.03 ** | 19.66 ± 0.92 ** |

** The specified values only were recorded in the pure PBAT polymer and was not associated with the bimodal melting temperatures of PHBV. Also, the calculated enthalpy corresponds to the PBAT crystallization process only.

diminished. On the other hand, the dispersion of the particles throughout the polymer matrix also had an impact on the crystallization properties. As the RS particles were immersed in the matrix, they decreased the crystallization capacity of the PHBV within the formulation and consequently the thermal properties were different.

### 3.7.2. Water vapor permeability (WVP)

On the other hand, as can be seen in Fig. 8B, the water vapor permeability showed similar behavior in the control formulations of 80:20 and 50:50. Particularly, there were non-significant differences after adding RS in the 80:20 formulation. In contrast, the WVP significantly increased after adding RS in the 50:50 formulation, almost doubling the permeability compared to the control. This indicates that the non-homogeneous and porous structure of the 50:50 formulation, as observed in Fig. 8A, likely facilitates the passage of water vapor through the material. Therefore, not only was the microstructure affected, but the permeability properties too, according to the type of polymeric blend.

Naturally, RS fibers are hydrophilic because of cellulose, and water can easily be absorbed in cellulose-based materials [51]. Therefore, the formation of micro-aggregates reduced the melt compounding capacity of the polymers, which consequently hindered the production of continuous films. Furthermore, these micro-spaces within the formulation potentially facilitated the transport of water vapor over time. Although the addition of RS was reported to increase the contact angle, suggesting a possible surface hydrophobicity, it is likely that after prolonged exposure in the water vapor permeability test, water diffusion through the material was more easily possible.

### 3.7.3. Disintegration and biodegradation analysis

The disintegration and biodegradation of polymer blends incorporating RS were evaluated using standardized methods. Disintegration tests, conducted according to ISO 20200:2016, revealed that only the 80:20 control and RS formulations met the standard, with disintegration percentages of 99.08 ± 0.22 % and 93.54 ± 0.71 %, respectively. The 50:50 formulations fell short of the standard, achieving 81.30 ± 4.99 % (control) and 87.67 ± 2.71 % (RS) disintegration. Notably, as shown in Fig. 8C, RS incorporation significantly enhanced degradation in the 50:50 formulations, while having minimal effect on 80:20 blends (Visual appearance shown in Fig. S6).

**Table 4**
DSC analysis (cold crystallization and melting) of polymers and composites by DSC during the second heating scan. Values with different superscript letters indicate significant differences as determined by ANOVA and Tukey test. Blank cells indicate cases where the values information was not applicable or detectable.

| PHBV:PBAT ratio | RS particle size | RS % | $T_{cc}$-PBAT (°C) | $\Delta H_{cc}$-PBAT (J/g) | $T_m$-PHBV-1 (°C) | $T_m$-PHBV-2 (°C) | $\Delta H_m$ (J/g) |
|---|---|---|---|---|---|---|---|
| | Control | 0 | – | – | 131.76 ± 0.00 $^{ab}$ | 168.08 ± 0.23 $^{ab}$ | 60.00 ± 1.03 $^{b}$ |
| | | 20 | – | – | 124.34 ± 0.37 $^{ab}$ | 162.39 ± 0.22 $^{cdef}$ | 35.76 ± 0.60 $^{e}$ |
| | ≤ 250 μm | 30 | – | – | 135.74 ± 0.78 $^{a}$ | 163.24 ± 0.05 $^{bcd}$ | 24.53 ± 0.27 $^{gh}$ |
| 80:20 | | 40 | – | – | 134.07 ± 0.55 $^{ab}$ | 158.92 ± 0.15 $^{defg}$ | 16.34 ± 0.14 $^{j}$ |
| | | 20 | – | – | 130.90 ± 0.43 $^{ab}$ | 160.41 ± 0.10 $^{defg}$ | 39.78 ± 1.35 $^{d}$ |
| | ≤ 500 μm | 30 | – | – | 134.30 ± 0.22 $^{a}$ | 162.95 ± 0.13 $^{bcde}$ | 24.17 ± 0.02 $^{gh}$ |
| | | 40 | – | – | 118.82 ± 6.50 $^{b}$ | 159.78 ± 1.11 $^{defg}$ | 16.22 ± 0.09 $^{j}$ |
| | Control | 0 | – | – | 125.74 ± 0.61 $^{ab}$ | 166.62 ± 0.13 $^{abc}$ | 47.91 ± 0.53 $^{c}$ |
| | | 20 | – | – | 124.59 ± 0.01 $^{ab}$ | 162.50 ± 0.08 $^{cdef}$ | 35.72 ± 0.33 $^{e}$ |
| | ≤ 250 μm | 30 | – | – | 135.51 ± 0.02 $^{a}$ | 162.31 ± 0.14 $^{cdef}$ | 18.58 ± 0.09 $^{i}$ |
| 50:50 | | 40 | – | – | 127.87 ± 7.15 $^{ab}$ | 156.81 ± 0.58 $^{g}$ | 12.94 ± 0.23 $^{kl}$ |
| | | 20 | – | – | 125.95 ± 0.98 $^{ab}$ | 162.41 ± 5.85 $^{cdef}$ | 28.91 ± 0.49 $^{f}$ |
| | ≤ 500 μm | 30 | – | – | 135.35 ± 0.90 $^{a}$ | 162.03 ± 0.26 $^{cdef}$ | 18.78 ± 0.08 $^{i}$ |
| | | 40 | – | – | 122.89 ± 0.17 $^{ab}$ | 157.91 ± 0.31 $^{efg}$ | 12.59 ± 0.44 $^{kl}$ |
| | Control | 0 | 45,68 ± 0,05 a | 4,68 ± 0,04 a | 123.87 ± 0.08 $^{ab}$ | 171.13 ± 0.10 $^{a}$ | 22.76 ± 0.08 $^{h}$ |
| | | 20 | 45,68 ± 0,05 a | 2,12 ± 0,14 b | 122.88 ± 0.46 $^{ab}$ | 163.23 ± 0.20 $^{bcd}$ | 15.93 ± 0.04 $^{j}$ |
| | ≤ 250 μm | 30 | 45,82 ± 0 a | 0,65 ± 0,01 d | 122.08 ± 0.20 $^{ab}$ | 159.47 ± 0.20 $^{defg}$ | 10.38 ± 0.38 $^{m}$ |
| 20:80 | | 40 | 46,08 ± 0,17 a | 0,16 ± 0,04 e | 131.25 ± 14.44 $^{ab}$ | 155.44 ± 0.02 $^{g}$ | 6.07 ± 0.76 $^{n}$ |
| | | 20 | 45,94 ± 0,45 a | 1,45 ± 0,01 c | 122.51 ± 0.60 $^{ab}$ | 163.52 ± 0.15 $^{bcd}$ | 13.45 ± 0.37 $^{k}$ |
| | ≤ 500 μm | 30 | 45,36 ± 0,17 a | 0,68 ± 0,11 d | 122.44 ± 0.99 $^{ab}$ | 160.17 ± 0.13 $^{defg}$ | 11.29 ± 0.22 $^{lm}$ |
| | | 40 | 44,16 ± 0,21 b | 0,28 ± 0,05 e | 122.41 ± 0.21 $^{ab}$ | 157.50 ± 0.21 $^{fg}$ | 7.28 ± 0.09 $^{n}$ |
| Neat PHBV | – | – | – | – | – | 170.23 ± 0.00 $^{a}$ | 102.55 ± 0.08 $^{a}$ |
| | | | | | **$T_m$-PBAT (°C)** | | |
| Neat PBAT | – | – | – | – | 116.63 ± 0.41 ** | – | 25.93 ± 0.77 ** |

** The specified values only were recorded in the pure PBAT polymer and was not associated with the bimodal melting temperatures of PHBV. Also, the calculated enthalpy corresponds to the PBAT melting process only.

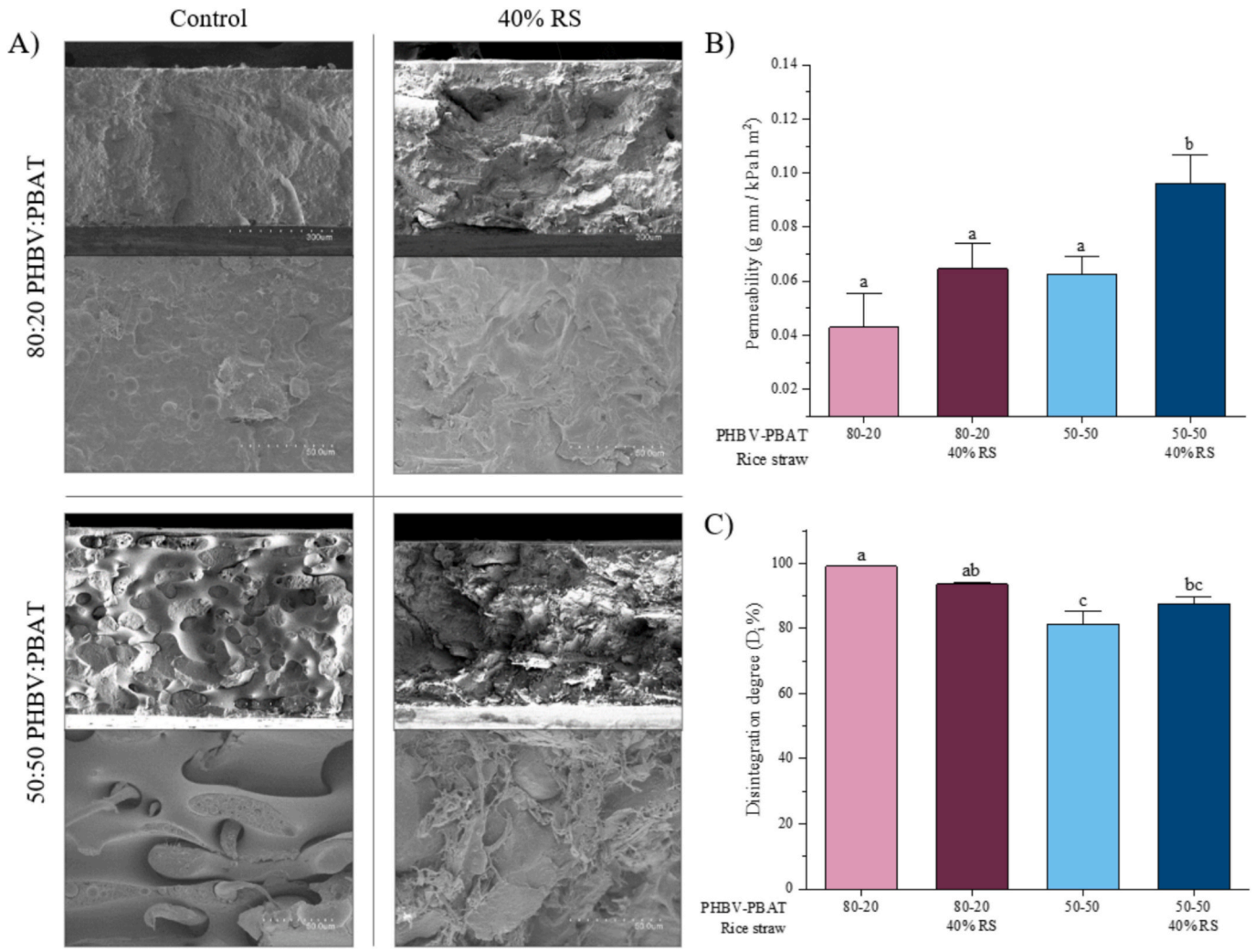


**Fig. 8.** Characterization of the control and 40 % RS formulations of the polymer blends 80:20 and 50:50. A) SEM images of the cross-section of the films after cryofracture, revealing globular-like formations, appearing as partially melted pellets that are physically connected yet still distinguish two distinct materials within the blend, resembling polymer inclusions dispersed throughout the other material. B) Water vapor permeability and C) Disintegration degree according to ISO 20200:2016.

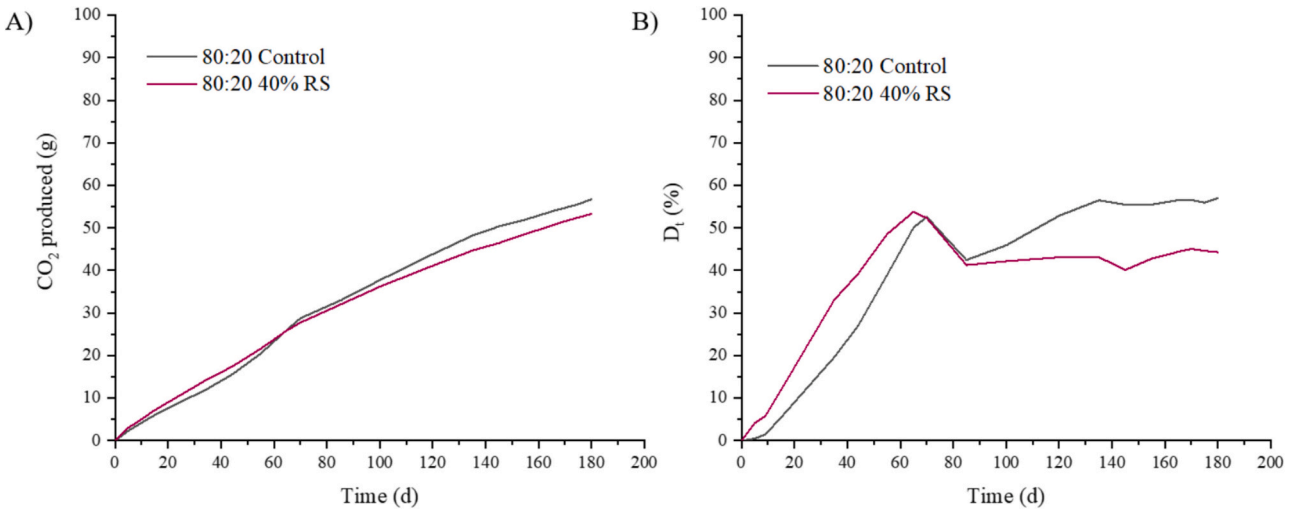


**Fig. 9.** Biodegradation of the 80:20 blend with and without RS load. A) Average $CO_2$ produced by the films and B) Biodegradation percentage over 180 days.

Subsequent biodegradation tests under industrial composting conditions (ISO 14855-2:2019) on the best-performing 80:20 formulations yielded unexpected results. Cumulative $CO_2$ emissions, indicative of material decomposition, reached 56.74 ± 2.80 g for the control and 53.33 ± 2.18 g for the 40 % RS formulation, as shown in Fig. 9. Biodegradation percentages followed a similar trend: 57.03 ± 13.66 % for the control and 44.32 ± 11.43 % for the RS formulation. Analogous results were obtained from home compost analysis, where the cumulative $CO_2$ emissions reached 49.50 ± 0.95 % for the control and 47.60 ± 0.98 for the RS formulation. Correspondingly, biodegradation percentage reached (38.98 ± 4.75 %) for the control and (36.10 ± 7.16 %) for the RS formulation. The lower performance of the RS formulation suggests that the recalcitrance of lignocellulosic biomass, particularly its high lignin content [26], hindered polymer degradation under these conditions. It has been reported that lignin is a complex polymer that is highly resistant to biodegradation [52].

The discrepancy between disintegration and biodegradation results can be attributed to several factors. The artificial substrate in the disintegration assay provided optimal conditions, whereas the natural compost in the biodegradation test presented challenges. This test discrepancy has been previously reported indicating a different behavior in the microbial communities; particularly, the heterogeneity of the compost between both assays might alter not only the microbial composition, but its evolution across the degradation process (lag, mesophilic, thermophilic and maturation phase). The diversity in the microbial communities (bacterial and fungal) decreased over composting, but its composition varies significantly in each phase. During both processes microbial communities evolve and get adapted to the different composting phases, resulting in drastic changes in the microbial succession [53].

Lignocellulosic biomasses like rice straw typically do not biodegrade efficiently in composting environments due to the lower abundance of specialized fungal species. Bacterial communities generally show higher diversity and abundance compared to fungal communities throughout the composting process [54]. Additionally, the microbial community has been reported to vary depending on the carbon and nitrogen sources such as paper, woodchips, manure, sludge, among others [55]. However, it has been reported that in open environments with high humidity and light exposure, similar composites the presence of the RS enhanced the fungal colonization and subsequent degradation. These fungi can induce cracking and degradation of RS/PHBV composites, potentially leading to faster degradation compared to the neat polymeric blend [56]. Also, the sample thickness might have limited the surface area accessible for microbial and enzymatic activity. In this respect, Pereira et al. (2024) [20] reported that the degradation of PHBV and PBAT, following the ASTM D6400 and NF EN 13432:2000 standards, was demonstrated to be compostable in-home compost conditions using films with thicknesses of 0.6 mm and 0.2 mm, respectively. Consequently, the thicker formulations as the ones developed in the present work, particularly those with a higher PBAT content, appear to be less susceptible to degradation under the specified conditions.

Furthermore, the hydrophilic components of rice straw could have affected moisture distribution and polymer-water interactions, further impacting the biodegradation process limiting the cleavage of ester bonds [57,58]. These findings underscore the complex interplay of factors influencing the degradation of RS-incorporated polymer blends and highlight the need for further optimization to enhance their biodegradability under various environmental conditions.

### 3.7.4. Environmental impact determination

The environmental impact of the PHBV:PBAT RS composite films were quantified by life cycle assessment (LCA) [59,60]. The complete life-cycle of the materials, considering the raw material sourcing, the energy consumption for processing (drying, milling, sieving, melt compounding, and compression molding), the end-of-life (EoL) treatment in an industrial composting facility, and the fossil-origin $CO_2$ emissions from composting are included in the assessment. Rice straw has been modeled following a zero-burden approach as it is considered a waste of rice production at harvest (the ISO 14044 defines a waste as a "substance or object which the holder intends or is required to dispose of") [61]. The transport of rice straw to the processing site and its conditioning for further processing is included. For conventional petroleum derived materials, municipal incineration has been set during the EoL phase. The climate change potential, expressed in $CO_2$ equivalents, is firstly analyzed given its ability to identify environmental hotspots during life-cycle stages, its relevance in the current climate crisis scenario, and its standardized character for comparison with similar materials [62]. As shown in Fig. 10A, the 80:20 40 % RS composite film has a total climate change potential of 7.89 kg $CO_2$-eq·kg$^{-1}$, while this value slightly increased to 8.28 kg $CO_2$-eq·kg$^{-1}$for the 50:50 40 % film. The largest contributors are the PHBV and PBAT, with a 44 % share in both compositions. In the case of these polymers, the conditioning (pellet drying) has a negligible contribution, while the transport to the processing site accounts for ~16 % of the contribution by the polymers. Besides, the RS has a minimal contribution (<0.1 %) because it is considered burden-free as obtained from waste streams (Fig. 10B), while the melt compounding and compression molding steps have a share of ~28 % and ~ 25 %, respectively. The low contribution of the EoL life-cycle stage in PHBV/PBAT/RS arises from its composting, which efficiently degrades bioplastics [63]. Besides, the degradation under aerobic conditions biologically oxidizes the carbon in the material to $CO_2$ (contrarily, under anaerobic conditions $CO_2$ and $CH_4$ are produced) [64], and solely the carbon from fossil origin is accounted as $CO_2$ emissions (0.12 and 0.30 kg $CO_2$-eq·kg$^{-1}$ for 80:20 40 % and 50:50 40 % formulations, respectively). In other words, the biogenic carbon is considered neutral in the carbon balance because the $CO_2$ released during composting was originally captured by the biomass during photosynthesis and plant growth. This agrees with the Product Environmental Footprint that solely considers $CO_2$ emissions from fossil origin at this life-cycle stage [21,63]. Contextualizing these values, Fig. 10C shows the *cradle-to-grave* climate change potential of five benchmark petroleum-derived plastic packaging films with an incineration EoL treatment. The results highlight the environmentally competitive character of PHBV/PBAT/RS composite films, with values that are below than most of the analyzed materials. Solely PVC scores better, while in the case of PLA it is necessary to have a biobased origin so the fossil $CO_2$ emissions during the end-of-life are avoided (3.71 kg $CO_2$-eq·kg$^{-1}$).

Additional impact categories have been also assessed to evaluate potential environmental trade-offs. As summarized in Fig. 11, the developed materials show values 2 to 5 times higher than the results obtained for commercial plastics. However, lower values are seen for the resource-related categories (metals/minerals and energy), suggesting the potential of these materials to develop a plastic packaging industry that is decoupled from the extensive use of finite resources. In this sense, it should be noted that the PHBV/PBAT/RS composite film have been developed at laboratory scale and that our calculations include a long transport of raw polymers (1405 km). In addition, a combination of laboratory-scale melt compounding and compression molding was used to form the composite film formation, which has a significantly larger footprint than industrial melt-extrusion processing of raw plastics. Additionally, while biocomposites made with RS may show higher land and water use than conventional plastics, they offer a sustainable alternative by repurposing agricultural residue. RS, often burned and wasted, is instead transformed into valuable materials. Since rice production, and thus straw generation, will continue to rise, this approach does not increase resource use but enhances environmental efficiency by reducing waste and emissions. Therefore, these values are promising, since by shortening supply chains and optimizing processing (reduced energy consumption to directly limit the impact on land and water use), it would be possible to obtain environmentally competitive materials. Overall, LCA findings clearly highlight the suitability of PHBV/PBAT/RS

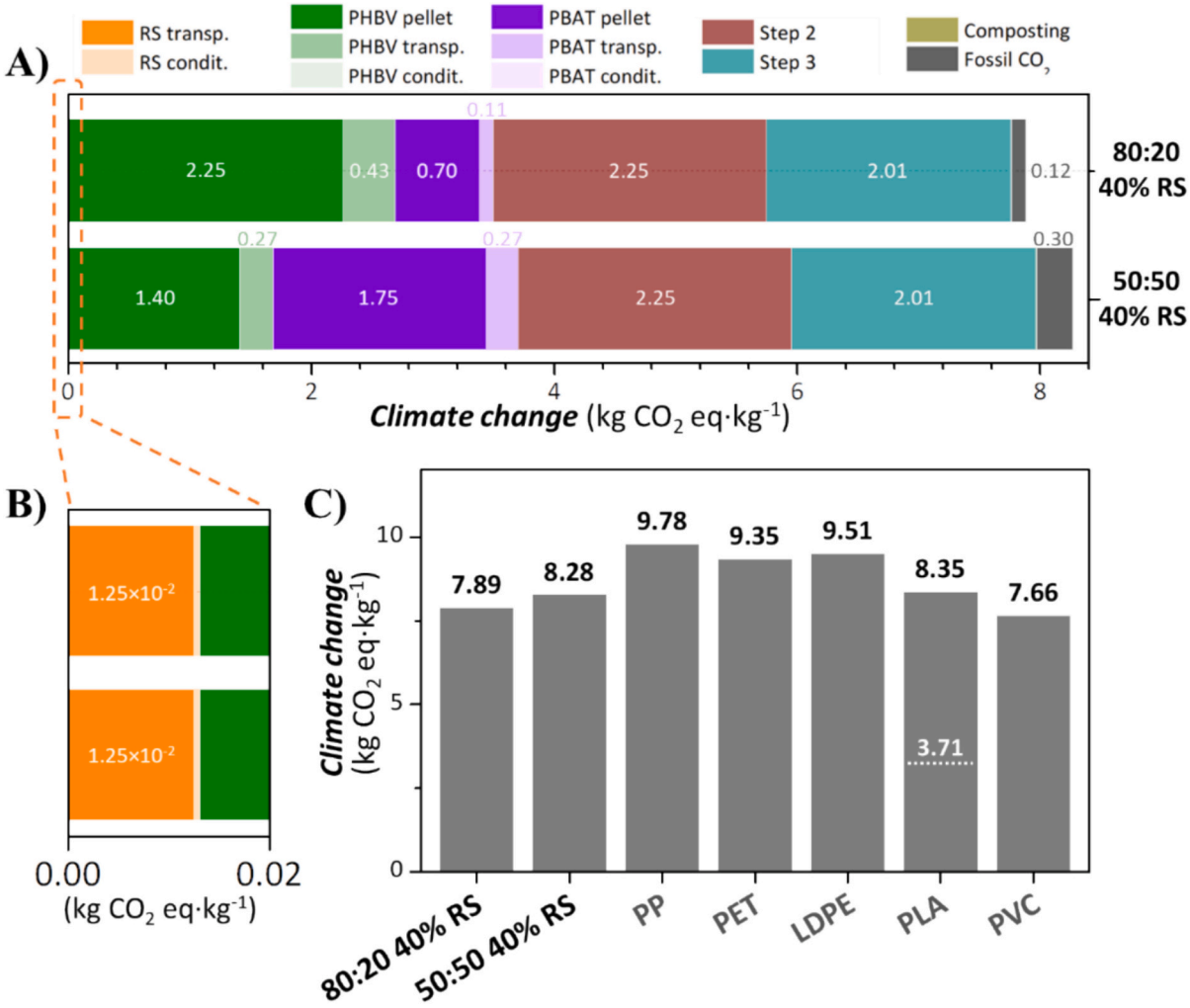


**Fig. 10.** A) Disaggregated *cradle-to-grave* climate change potential per kilogram of composite film, with specific contributions expressed in kg $CO_2$-eq·$kg^{-1}$; B) a magnified view of to show the contribution of rice straw. C) Total *cradle-to-grave* climate change potential per kilogram of composite film compared to benchmark packaging plastics. The assessment includes film production, the treatment of waste plastic by municipal incineration, and fossil $CO_2$ emissions. PP: polypropylene; PET: polyethylene terephthalate; LDPE: low-density polyethylene; PLA: polylactic acid; PVC: polyvinyl chloride. The white line represents the *cradle-to-grave* impact for a bio-based PLA having a composting EoL and no fossil $CO_2$ emissions upon degradation (3.71 kg $CO_2$-eq·$kg^{-1}$).

to develop environmentally sustainable products for the packaging field.

## 4. Conclusions

The present work investigates the impact of rice straw incorporation on PHBV:PBAT blend composites, demonstrating significant effects on colorimetric, hydrophobic, mechanical, thermal, microstructural, and degradation properties. The PHBV:PBAT ratio determined the fundamental properties of the material (mechanical and thermal properties, and disintegration capacity). For instance, the greater the PHBV content, the higher the rigidity and the less ductility. Also, the 80:20 composites showed the highest significant increment in Young's modulus (35 % higher), indicating better compatibility of the RS with the PHBV. On the other hand, the 20:80 formulation showed higher tensile strength proportionally with the RS content, suggesting that adding the RS did not represent significant strength loss.

Regarding the contact angle, the 80:20 blend showed a higher improvement in hydrophobicity after RS addition. Consequently, the barrier properties of the 80:20 formulation were better than those of the 50:50 formulation. Nevertheless, the addition of RS decreased the barrier capacity of the materials. Regarding the particle size variable, it showed influence in the optical properties and the RS-reinforcement properties evaluated in mechanical testing. Thus, the ≤250 μm particle use resulted in greater color changes than ≤500 μm at the same concentration, suggesting that small particles allowed a homogeneous dispersion within the polymer matrix; hence, the particle size also affected the water contact angle results. The polymer crystallization was not affected by the particle size. Concerning the RS concentration variable, it enhanced the color change, improved the rigidity, decreased the elongation at break, increased the tensile strength, decreased the thermal stability, and hindered polymer crystallization. In particular, it directly impacted the color change, where the higher the RS concentration, the higher the color change, and the darker and duller the films. Also, the ductility was reduced with the RS addition and had an important effect in the reinforcement effect, which was also directly proportional.

Disintegration tests (ISO 20200:2016) showed that only the 80:20 blends met the standard, with RS enhancing degradation in 50:50 formulations. Biodegradation tests (ISO 14855-2:2019) under industrial composting conditions revealed lower biodegradation percentages for the RS-containing 80:20 blend compared to the control, likely due to the recalcitrance of lignin in RS. The discrepancy between disintegration and biodegradation highlights the influence of environmental conditions and microbial communities on RS-incorporated polymer degradation. A *cradle-to-grave* life cycle assessment reveals a climate change potential of 7.89–8.28 kg $CO_2$-eq per kilogram of PHBV/PBAT/RS film.

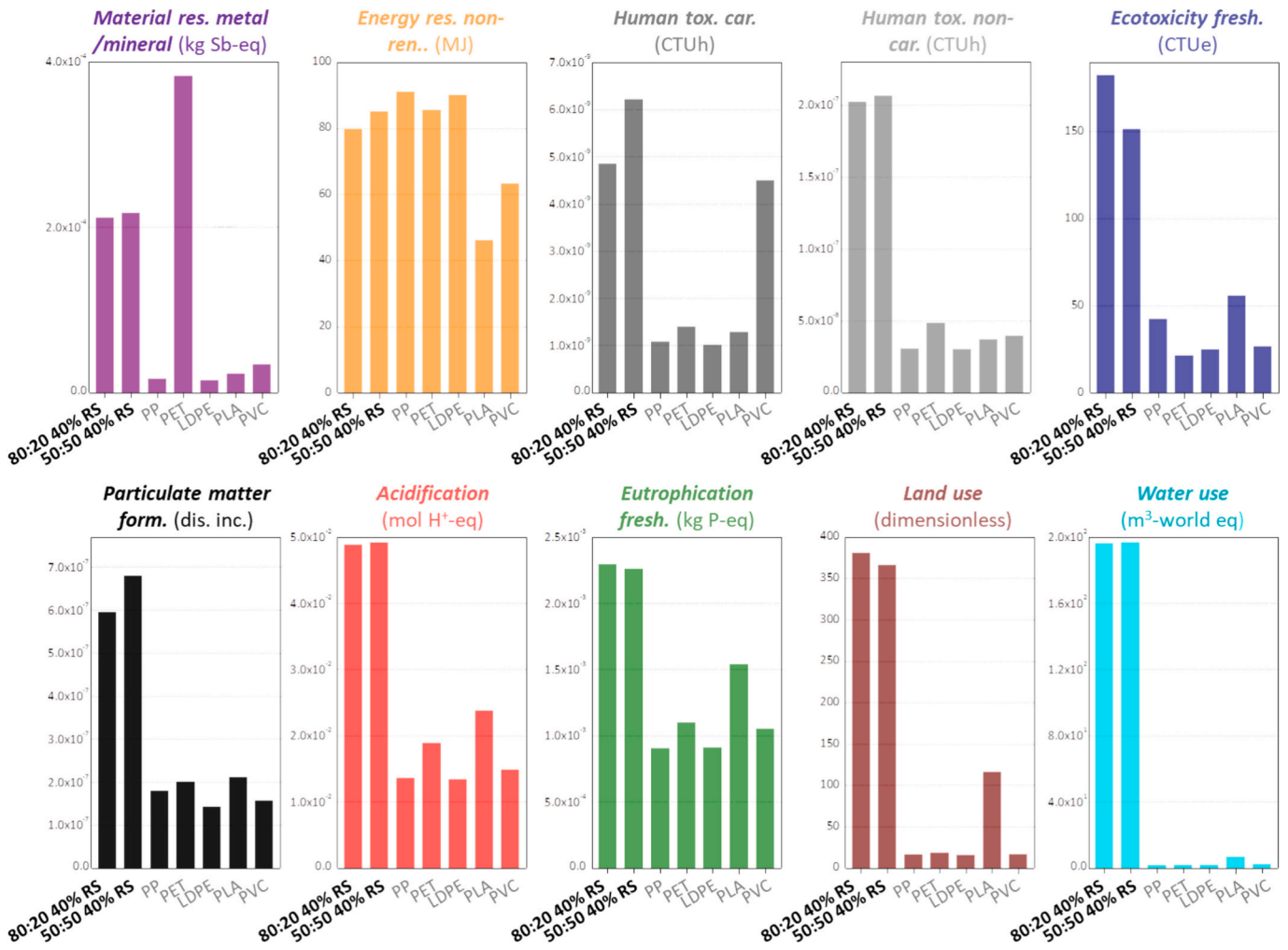


**Fig. 11.** Environmental impacts in ten relevant indicators according to the Environmental Footprint 3.1 impact assessment methodology. The results are compared with the impacts obtained for five competitive packaging materials. Where the abbreviations stand for rice straw (RS), polypropylene (PP), polyethylene terephthalate (PET), polyethylene (PE), polylactic acid (PLA) and polyvinyl chloride (PVC).

Such values are comparable to, or even lower than, the *cradle-to-grave* climate change potential shown by the benchmark petroleum-derived packaging films with a mature supply chain and processing processes, which fall between 7.66 and 9.78 kg CO2-eq·kg$^{-1}$. The PHBV/PBAT/RS composite films also score lower in additional impact categories, proving the potential of organic waste such as RS for sustainable bio-product development. These findings provide valuable insights into the potential of RS as a sustainable filler in biodegradable polymer composites for packaging applications.

## CRediT authorship contribution statement

**Laura Cabrera-Villamizar:** Writing – original draft, Investigation, Formal analysis, Data curation, Conceptualization. **Eugenia Núñez:** Writing – review & editing, Methodology, Formal analysis, Data curation. **Alcira Reyes:** Methodology, Investigation, Formal analysis, Data curation. **Erlantz Lizundia:** Writing – review & editing, Visualization, Software, Methodology, Formal analysis. **Amparo López-Rubio:** Writing – review & editing, Supervision, Project administration, Funding acquisition, Conceptualization. **María José Fabra:** Writing – review & editing, Supervision, Project administration, Methodology, Funding acquisition, Conceptualization.

## Declaration of competing interest

The authors declare that there are no conflicts of interest.

## Acknowledgements

Grants PID2023-146557OB-C22 funded by MICIU/AEI/ 10.13039/501100011033 and, by ERDF A way of making Europe. The EVOLVE-PACK project (Innovative Sustainable Packaging to Safeguard Our Food and Our Planet) is a contribution to PRIMA program (Partnership for Research and Innovation in the Mediterranean Area) funded by the European Union Horizon 2020 program and national research funding agency (PCI2024-153409). Laura Cabrera-Villamizar acknowledges financial support from the Generalitat Valenciana for the award of a Santiago Grisolía grant (GRISOLIA/2021/050). EL acknowledges financial support from the University of the Basque Country (Convocatoria de ayudas a grupos de investigación GIU21/010). The Accreditation as Center of Excellence Severo Ochoa CEX2021-01189-S funded by MCIN/AEI / 10.13039/501100011033 is also fully acknowledged.

## Appendix A. Supplementary data

Supplementary data to this article can be found online at https://doi.org/10.1016/j.ijbiomac.2025.146804.

## Data availability

Data will be made available on request.

## References


[1] A.K. Singh, R. Bedi, A. Khajuria, A review of composite materials based on rice straw and future trends for sustainable composites, J. Clean. Prod. 457 (Jun. 2024) 142417, https://doi.org/10.1016/j.jclepro.2024.142417.

[2] D. de Gómez Barreda, et al., An overview of rice cultivation in Spain and the management of herbicide-resistant weeds, Agronomy 11 (6) (2021) 1095, https://doi.org/10.3390/agronomy11061095.

[3] A. Quintana-Gallardo, J. Romero Clausell, I. Guillén-Guillamón, F.A. Mendiguchia, Waste valorization of rice straw as a building material in Valencia and its implications for local and global ecosystems, J. Clean. Prod. 318 (Oct. 2021) 128507, https://doi.org/10.1016/j.jclepro.2021.128507.

[4] A.C.F. Louis, S. Venkatachalam, S. Gupta, Innovative strategy for rice straw valorization into nanocellulose and nanohemicellulose and its application, Ind. Crops Prod. 179 (2022) 114695, https://doi.org/10.1016/j.indcrop.2022.114695.

[5] N.T. Vo, C.D. Pham, T.B. Ly, M.D.T. Dang, N.H.N. Do, P.K. Le, Valorization of rice straw for valuable materials: towards a zero-waste recovery process, Biomass Convers. Biorefin. 14 (23) (Dec. 2024) 29901–29910, https://doi.org/10.1007/s13399-023-04681-0.

[6] S. Singh, G. Kaur, D.P. Singh, S.K. Arya, M. Krishania, Exploring rice straw's potential from a sustainable biorefinery standpoint: towards valorization and diverse product production, Process Saf. Environ. Prot. 184 (Apr. 2024) 314–331, https://doi.org/10.1016/j.psep.2024.01.105.

[7] S. Sharma, A. Pappu, S.R. Asolekar, Sustainable recycling of paddy straw through development of short-fiber-reinforced composites: exploring gainful utilization of agricultural waste, Clean Techn. Environ. Policy. 26 (1) (2024) 109–127, https://doi.org/10.1007/s10098-023-02607-y.

[8] Somvanshi, K. S., Gope, P. C., and S., T. A review on properties of nano biocomposite film for packaging applications from cellulose nano fiber. Int. J. Eng. Res. Appl., 11, 1, 29-39.

[9] Q. Yang, et al., Effect of chemical treatment on rice straw fiber surface and properties of straw/polylactic acid composites, J. Nat. Fibers 20 (2) (Nov. 2023), https://doi.org/10.1080/15440478.2023.2228486.

[10] A. Allahbakhsh, PVC/rice straw/SDBS-modified graphene oxide sustainable nanocomposites: melt mixing process and electrical insulation characteristics, Compos. Part A Appl. Sci. Manuf. 134 (Jul. 2020) 105902, https://doi.org/10.1016/j.compositesa.2020.105902.

[11] M. Megahed, S.S. Ali-Eldin, S.M. Abd El Moezz, W. Abdalla, Synthesis of developed rice straw sheets and glass fiber-reinforced polyester composites, J. Compos. Mater. 54 (23) (Sep. 2020) 3381–3394, https://doi.org/10.1177/0021998320915641.

[12] J. Liu, H. Su, L. Guo, M. Zhang, Environmentally sound materials from rice straw for elevator decoration, J. Phys. Conf. Ser. 1545 (1) (2020) 012004, https://doi.org/10.1088/1742-6596/1545/1/012004.

[13] B. Dushyanthini, V.P.S. Perera, J.C.N. Rajendra, N. Karthikeyan, G.K.R. Senadeera, Composite materials based on rice straw and natural rubber for thermal insulation applications, Ceylon J. Sci. 52 (2) (2023) 155–161, https://doi.org/10.4038/cjs.v52i2.8157.

[14] F. Kundie, C.H. Azhari, A. Muchtar, Z.A. Ahmad, Effects of filler size on the mechanical properties of polymer-filled dental composites: a review of recent developments, J. Phys. Sci. 29 (1) (2018) 141–165, https://doi.org/10.21315/jps2018.29.1.10.

[15] Y.W. Sitotaw, N.G. Habtu, A.Y. Gebreyohannes, S.P. Nunes, T. Van Gerven, Ball milling as an important pretreatment technique in lignocellulose biorefineries: a review, Biomass Convers. Biorefinery 13 (17) (Nov. 2023) 15593–15616, https://doi.org/10.1007/s13399-021-01800-7.

[16] I. Naghmouchi, F.X. Espinach, P. Mutjé, S. Boufi, Polypropylene composites based on lignocellulosic fillers: how the filler morphology affects the composite properties, Mater. Des. (1980-2015) 65 (2015) 454–461, https://doi.org/10.1016/j.matdes.2014.09.047.

[17] Y. Zare, Study of nanoparticles aggregation/agglomeration in polymer particulate nanocomposites by mechanical properties, Compos. Part A Appl. Sci. Manuf. 84 (May 2016) 158–164, https://doi.org/10.1016/j.compositesa.2016.01.020.

[18] G. Policastro, A. Panico, M. Fabbricino, Improving biological production of poly(3-hydroxybutyrate-co-3-hydroxyvalerate) (PHBV) co-polymer: a critical review, Rev. Environ. Sci. Biotechnol. 20 (2) (2021) 479–513, https://doi.org/10.1007/s11157-021-09575-z.

[19] V. Jost, H.-C. Langowski, Effect of different plasticisers on the mechanical and barrier properties of extruded cast PHBV films, Eur. Polym. J. 68 (Jul. 2015) 302–312, https://doi.org/10.1016/j.eurpolymj.2015.04.012.

[20] J.F. Pereira, E. Núñez, A. Reyes, S. Mali, A. Lopez-Rubio, M.J. Fabra, On the use of lignocellulosic hemp fibers to produce biodegradable cost-efficient biocomposites, Future Foods 10 (Dec. 2024) 100507, https://doi.org/10.1016/j.fufo.2024.100507.

[21] R. Garcia, F. Freire, Carbon footprint of particleboard: a comparison between ISO/TS 14067, GHG protocol, PAS 2050 and climate declaration, J. Clean. Prod. 66 (Mar. 2014) 199–209, https://doi.org/10.1016/j.jclepro.2013.11.073.

[22] J. Huang, S. Wang, J. Chen, C. Chen, E. Lizundia, Environmental sustainability of natural biopolymer-based electrolytes for lithium ion battery applications, Adv. Mater. 37 (22) (2025), https://doi.org/10.1002/adma.202416733.

[23] L. Chen, et al., Biomass waste-assisted micro(nano)plastics capture, utilization, and storage for sustainable water remediation, The Innovation 5 (4) (Jul. 2024) 100655, https://doi.org/10.1016/j.xinn.2024.100655.

[24] P.F. Sommerhuber, J.L. Wenker, S. Rüter, A. Krause, Life cycle assessment of wood-plastic composites: Analysing alternative materials and identifying an environmental sound end-of-life option, Resour. Conserv. Recycl. 117 (Feb. 2017) 235–248, https://doi.org/10.1016/j.resconrec.2016.10.012.

[25] R.L. de Lapuente Díaz de Otazu, O. Akizu-Gardoki, B. de Ulibarri, M. Iturrondobeitia, R. Minguez, E. Lizundia, Ecodesign coupled with life cycle assessment to reduce the environmental impacts of an industrial enzymatic cleaner, Sustain. Prod. Consum. 29 (Jan. 2022) 718–729, https://doi.org/10.1016/j.spc.2021.11.016.

[26] L.A. Cabrera-Villamizar, M. Ebrahimi, A. Martínez-Abad, D. Talens-Perales, A. López-Rubio, M.J. Fabra, Order matters: methods for extracting cellulose from rice straw by coupling alkaline, ozone and enzymatic treatments, Carbohydr. Polym. 328 (Mar. 2024) 121746, https://doi.org/10.1016/j.carbpol.2023.121746.

[27] P.A.V. Freitas, C. González-Martínez, A. Chiralt, Antioxidant starch composite films containing rice straw extract and cellulose fibres, Food Chem. 400 (Jan. 2023) 134073, https://doi.org/10.1016/j.foodchem.2022.134073.

[28] L. Cabrera-Villamizar, J.F. Pereira, M. Castanedo, A. López-Rubio, M.J. Fabra, Hemp cellulose-based aerogels and cryogels: from waste biomass to sustainable absorbent pads for food preservation, Carbohydr. Polym. 348 (Jan. 2025) 122887, https://doi.org/10.1016/j.carbpol.2024.122887.

[29] Z. Pérez-Bassart, A. Reyes, A. Martínez-Abad, A. López-Rubio, M.J. Fabra, Feasibility of Agaricus bisporus waste biomass to develop biodegradable food packaging materials, Food Hydrocoll. 142 (Sep. 2023) 108861, https://doi.org/10.1016/j.foodhyd.2023.108861.

[30] M.J. Fabra, G. Sánchez, A. López-Rubio, J.M. Lagaron, Microbiological and ageing performance of polyhydroxyalkanoate-based multilayer structures of interest in food packaging, LWT Food Sci. Technol. 59 (2) (Dec. 2014) 760–767, https://doi.org/10.1016/j.lwt.2014.07.021.

[31] A. Martínez-Abad, J. González-Ausejo, J.M. Lagarón, L. Cabedo, Biodegradable poly(3-hydroxybutyrate-co-3-hydroxyvalerate)/thermoplastic polyurethane blends with improved mechanical and barrier performance, Polym. Degrad. Stab. 132 (Oct. 2016) 52–61, https://doi.org/10.1016/j.polymdegradstab.2016.03.039.

[32] R.R.A. Silva, C.S. Marques, T.R. Arruda, S.C. Teixeira, T.V. de Oliveira, Biodegradation of polymers: stages, measurement, standards and prospects, Macromol 3 (2) (2023) 371–399, https://doi.org/10.3390/macromol3020023.

[33] D.K. Giang, et al., Effect of torrefied biomass on hydrophobicity and mechanical properties of polylactic acid composite, Int. J. Biol. Macromol. 215 (Aug. 2022) 36–44, https://doi.org/10.1016/j.ijbiomac.2022.06.084.

[34] V. Arumugaprabu, R.D.J. Johnson, S. Vigneshwaran, Mechanical performance of nanocomposites and biomass-based composite materials and its applications: An overview, in: Handbook of Nanomaterials and Nanocomposites for Energy and Environmental Applications, Springer International Publishing, Cham, 2021, pp. 991–1004, https://doi.org/10.1007/978-3-030-36268-3_123.

[35] P. Zytner, A.K. Pal, F. Wu, A. Rodriguez-Uribe, A.K. Mohanty, M. Misra, Morphology and performance relationship studies on poly(3-hydroxybutyrate- *co* −3-hydroxyvalerate)/poly(butylene adipate- *co* -terephthalate)-based biodegradable blends, ACS Omega 8 (2) (Jan. 2023) 1946–1956, https://doi.org/10.1021/acsomega.2c04770.

[36] M.J. Rosado, G. Marques, J. Rencoret, A. Gutiérrez, J.C. del Río, Chemical composition of lipophilic compounds from rice (Oryza sativa) straw: an attractive feedstock for obtaining valuable phytochemicals, Front. Plant Sci. 13 (Mar. 2022), https://doi.org/10.3389/fpls.2022.868319.

[37] J. Ruwoldt, F.H. Blindheim, G. Chinga-Carrasco, Functional surfaces, films, and coatings with lignin – a critical review, RSC Adv. 13 (18) (2023) 12529–12553, https://doi.org/10.1039/D2RA08179B.

[38] S.P. Pawar, A. Misra, S. Bose, K. Chatterjee, V. Mittal, Enzymatically degradable and flexible bio-nanocomposites derived from PHBV and PBAT blend: assessing thermal, morphological, mechanical, and biodegradation properties, Colloid Polym. Sci. 293 (10) (Oct. 2015) 2921–2930, https://doi.org/10.1007/s00396-015-3700-y.

[39] A.K. Pal, M. Misra, A.K. Mohanty, Silane treated starch dispersed PBAT/PHBV-based composites: improved barrier performance for single-use plastic alternatives, Int. J. Biol. Macromol. 229 (Feb. 2023) 1009–1022, https://doi.org/10.1016/j.ijbiomac.2022.12.141.

[40] E. Moll, A. Chiralt, Polyhydroxybutyrate-co-hydroxyvalerate (PHBV) with phenolic acids for active food packaging, Polymers (Basel) 15 (21) (2023) 4222, https://doi.org/10.3390/polym15214222.

[41] A. Gupta, L. Lolic, T.H. Mekonnen, Reactive extrusion of highly filled, compatibilized, and sustainable PHBV/PBAT – hemp residue biocomposite, Compos. Part A Appl. Sci. Manuf. 156 (May 2022) 106885, https://doi.org/10.1016/j.compositesa.2022.106885.

[42] Y. Kann, M. Shurgalin, R.K. Krishnaswamy, FTIR spectroscopy for analysis of crystallinity of poly(3-hydroxybutyrate-co-4 -hydroxybutyrate) polymers and its utilization in evaluation of aging, orientation and composition, Polym. Test. 40 (Dec. 2014) 218–224, https://doi.org/10.1016/j.polymertesting.2014.09.009.

[43] Y. Cai, J. Lv, J. Feng, Spectral characterization of four kinds of biodegradable plastics: poly (lactic acid), poly (Butylenes Adipate-co-terephthalate), poly (Hydroxybutyrate-co-Hydroxyvalerate) and poly (Butylenes succinate) with FTIR and Raman spectroscopy, J. Polym. Environ. 21 (1) (Mar. 2013) 108–114, https://doi.org/10.1007/s10924-012-0534-2.

[44] Y.-M. Corre, S. Bruzaud, J.-L. Audic, Y. Grohens, Morphology and functional properties of commercial polyhydroxyalkanoates: a comprehensive and

comparative study, Polym. Test. 31 (2) (Apr. 2012) 226–235, https://doi.org/10.1016/j.polymertesting.2011.11.002.
[45] I. Zembouai, et al., Poly(3-Hydroxybutyrate-co-3-Hydroxyvalerate)/Polylactide blends: thermal stability, flammability and Thermo-mechanical behavior, J. Polym. Environ. 22 (1) (Mar. 2014) 131–139, https://doi.org/10.1007/s10924-013-0626-7.
[46] Z. Zaidi, A. Crosky, Unidirectional rubber-toughened green composites based on PHBV, Sustainability 11 (8) (Apr. 2019) 2411, https://doi.org/10.3390/su11082411.
[47] M. Bianchi, A. Dorigato, M. Morreale, A. Pegoretti, Evaluation of the physical and shape memory properties of fully biodegradable poly(lactic acid) (PLA)/poly (butylene adipate terephthalate) (PBAT) blends, Polymers 15 (4) (2023) 881, https://doi.org/10.3390/polym15040881.
[48] W. Zhang, Q. Wang, G. Wang, S. Liu, Synthesis and characterization of bio-based poly(ethylene 2,5-furandicarboxylate)-b-poly(butylene adipate-co-terephthalate) copolymers, J. Appl. Polym. Sci. 139 (34) (Sep. 2022), https://doi.org/10.1002/app.52803.
[49] N. Tomano, O. Boondamnoen, C. Aumnate, P. Potiyaraj, Enhancing impact resistance and biodegradability of PHBV by melt blending with ENR, Sci. Rep. 12 (1) (Dec. 2022) 22633, https://doi.org/10.1038/s41598-022-27246-z.
[50] Y. Qin, G. Jiang, Q. Xu, P. Li, S. Wei, J. Liu, Preparation of poly(3-hydroxybutyrate-co-3-hydroxy-valerate) (PHBV)-based composites using poly(butylene adipate-co-terephthalate) (PBAT) and bagasse, Bioresources 17 (3) (May 2022) 4136–4150, https://doi.org/10.15376/biores.17.3.4136-4150.
[51] I.R.S. Daulay, et al., Preparation of superhydrophobic biomedical pulp from rice straw coated with a stearic acid-cellulose composite, Bioresour. Technol. Rep. 25 (Feb. 2024) 101781, https://doi.org/10.1016/j.biteb.2024.101781.
[52] F. Al-Dhabaan, Safety disposal of rice straw by biodegradation using *Streptomyces tendae*, Sustainability 13 (24) (2021) 13640, https://doi.org/10.3390/su132413640.
[53] J. Wan, et al., Livestock manure type affects microbial community composition and assembly during composting, Front. Microbiol. 12 (Mar. 2021), https://doi.org/10.3389/fmicb.2021.621126.
[54] S. Pot, et al., Understanding the shift in the microbiome of composts that are optimized for a better fit-for-purpose in growing media, Front. Microbiol. 12 (Apr. 2021), https://doi.org/10.3389/fmicb.2021.643679.
[55] D.A. Neher, T.R. Weicht, S.T. Bates, J.W. Leff, N. Fierer, Changes in bacterial and fungal communities across compost recipes, preparation methods, and composting times, PloS One 8 (11) (Nov. 2013) e79512, https://doi.org/10.1371/journal.pone.0079512.
[56] N.D. Yaacob, S. Sung Ting, A.M. Azizul Rashidi, Natural weathering degradation studies of the poly (3-hydroxybutyrate-co-3 hydroxyvalerate) (PHBV)/paddy straw powder (PSP) biocomposites, Progress in Rubber, Plastics and Recycling Technology 41 (2) (May 2025) 127–143, https://doi.org/10.1177/14777606241257063.
[57] M. Fernandes, A.F. Salvador, D.A. Madalena, A.A. Vicente, Estimating the biodegradation of PHB/PBAT films – an experimental design approach, 2024, https://doi.org/10.2139/ssrn.4888278.
[58] M. Fogašová, et al., PLA/PHB-based materials fully biodegradable under both industrial and home-composting conditions, Polymers (Basel) 14 (19) (2022) 4113, https://doi.org/10.3390/polym14194113.
[59] M. Iturrondobeitia, O. Akizu-Gardoki, R. Minguez, E. Lizundia, Environmental impact analysis of aprotic Li–O $_2$ batteries based on life cycle assessment, ACS Sustain. Chem. Eng. 9 (20) (May 2021) 7139–7153, https://doi.org/10.1021/acssuschemeng.1c01554.
[60] J.F. Peters, Best practices for life cycle assessment of batteries, Nat. Sustain. 6 (6) (Feb. 2023) 614–616, https://doi.org/10.1038/s41893-023-01067-y.
[61] D. Dominguez Aldama, F. Grassauer, Y. Zhu, A. Ardestani-Jaafari, N. Pelletier, Allocation methods in life cycle assessments (LCAs) of agri-food co-products and food waste valorization systems: systematic review and recommendations, J. Clean. Prod. 421 (Oct. 2023) 138488, https://doi.org/10.1016/j.jclepro.2023.138488.
[62] S. Fankhauser, et al., The meaning of net zero and how to get it right, Nat. Clim. Chang. 12 (1) (2022) 15–21, https://doi.org/10.1038/s41558-021-01245-w.
[63] A. Keyes, C.M. Saffron, S. Manjure, R. Narayan, Biobased compostable plastics end-of-life: environmental assessment including carbon footprint and microplastic impacts, Polymers (Basel) 16 (21) (2024) 3073, https://doi.org/10.3390/polym16213073.
[64] R. Narayan, Carbon footprint of bioplastics using biocarbon content analysis and life-cycle assessment, MRS Bull. 36 (9) (Sep. 2011) 716–721, https://doi.org/10.1557/mrs.2011.210.